Beyond environmental monitoring: Are automatic time-lapse cameras efficient tools for temperature measurement in remote regions?

Jérémy Grenier, Armelle Decaulne, Najat Bhiry

Beyond environmental monitoring: Are automatic time-lapse cameras efficient tools for temperature measurement in remote regions?

Au-delà de la surveillance environnementale : est-ce que les appareils photographiques automatisés sont un outil efficace pour la mesure de température en régions éloignées ?

Jérémy Grenier [a*], Armelle Decaulne [b], Najat Bhiry [a]

[a] Département de géographie et Centre d'études nordiques, Université Laval, Québec, G1V 0A6, Canada.
[b] CNRS, LETG-Nantes UMR 6554, Institut de géographie et d'aménagement de l'université de Nantes (IGARUN), Nantes Université, Campus du Tertre BP 81227, 44312 Nantes, France.

ABSTRACT

Automatic time-lapse cameras are frequently used to monitor snow height as well as snow and ice related processes occurring on slopes in cold regions because of the many advantages they bring to researchers. In addition to providing important visual information's about the dynamic of the studied area, most of these types of cameras are now equipped with thermal sensors able to register temperature data for every picture taken. The instrumentation set up within Tasiapik Valley, near Umiujaq, in Nunavik (northern Québec), enabled us to assess the potential of automatic time-lapse cameras for temperature measurement by comparing data retrieved on photographs from time-lapse cameras with data from two nearby weather stations. Our results indicate that the temperature measurements from the time-lapse cameras from August to the onset of February are relatively accurate while their weaker performances for temperature measurement occurred in late winter and spring (March - June). Moreover, regardless of the year, time-lapse cameras were most accurate in the morning (09:00 AM – 11:00 AM), while in the afternoon (12:00 PM – 3:00 PM), they tended to over-estimate temperatures. Based on our observations and data analyses, this over-estimation of temperatures seems to be caused by external factors such as sky conditions and high values of downwelling shortwave radiation lasting from February to June at our study site. The local environment surrounding the cameras might also affect the performances of time-lapse cameras at temperature measurement.

Keywords: temperature data, time-lapse cameras, weather station, data reliability.

RÉSUMÉ

Les appareils photographiques automatisés sont fréquemment utilisés pour surveiller la hauteur de neige ainsi que les processus liés à la neige et à la glace qui se produisent sur les pentes de régions froides en raison des nombreux avantages qu'ils apportent aux chercheurs. En plus de prodiguer d'importantes informations visuelles sur la dynamique du site à l'étude, la plupart des modèles d'appareil photographique automatisé est désormais doté de capteurs thermiques permettant l'enregistrement d'une valeur de température pour chaque photographie capturée. L'instrumentation de la Vallée Tasiapik, en marge du village d'Umiujaq, au Nunavik (Nord-du-Québec), nous as permis d'évaluer le potentiel des appareils photographiques automatisés pour la mesure de température en comparant les valeurs de températures enregistrées par les appareils photographiques à celles enregistrées par deux stations météorologiques situées à proximité. Les résultats indiquent que les mesures de température réalisées par les appareils photographiques entre les mois d'aout jusqu'au début de mois de février sont relativement précises tandis que les performances les plus faibles ont eu lieu à la fin de l'hiver et au printemps (mars - juin). De plus, quelle que soit l'année, les appareils photographiques automatisés étaient plus précis en début de journée (09h00 – 11h00), tandis qu'en après-midi (12h00 – 15h00), ils avaient tendance à surestimer beaucoup les températures. D'après nos observations et l'analyse des données, cette surestimation des températures semble être causée par des facteurs externes tels que les conditions du ciel et les valeurs élevées du rayonnement solaire présente de février à juin sur notre site d'étude. L'environnement local à proximité des caméras pourrait également affecter les performances des appareils photographiques en matière de mesure de température.

Mots-clés : *données de température, appareils photographiques automatisés, station météorologique, fiabilité des données.*

1. Introduction

Automatic time-lapse cameras were frequently used in recent years to monitor snow and/or ice related slope processes in cold regions. They were used notably by Gauthier et al. (2012) in the Chics-Chocs (Eastern Canada); Peitzsch et al. (2012), and Munroe (2018) in the Western United States; Eckerstorfer et al. (2013a,b) in Svalbard; van Herwijinen et al. (2013), van Herwijinen and Fierz (2014), and Dreier et al. (2016) in the Swiss Alps, Laute and Beylich (2014, 2018) in mainland Norway; Abermann et al. (2019) in Greenland; Dufour-Beauséjour et al. (2020), Veilleux et al., (2021), and Grenier et al. (2023) in Nunavik. This remote sensing method has gained popularity in the last decade mostly because of the many advantages it brings to researchers, such as covering difficultly

accessible terrain, the possibility to acquire complete data records for a location over a given time frame, and thus, without altering the physical properties of the studied objects, for example the snow cover, in addition to providing a safe observer position (Eckerstorfer et al., 2016).

However, apart from providing visual qualitative information concerning the studied processes and the weather conditions within the observable area (*e.g.,* cloudy, sunny, windy conditions), most of these types of cameras are now equipped with thermal sensors able to provide temperature data for every picture taken. Users of such cameras frequently protect them in weather/animal-proof metallic cases to ensure their data is safe from any possible hazard. This practice has for effect that the cameras sensors might be affected by external factors such as incident solar radiation which is dependant on the cloud coverage present at the time of each temperature measurement. Therefore, researchers usually rely on data from the closest available weather station, which can sometimes be located as far as a hundred kilometers away from the site of interest, to get weather data. This method might be problematic when monitoring remote regions since *(i)* weather conditions might be completely different from the study area and *(ii)* the setting of a weather station near study area can be very onerous (Pigeon and Jiskoot, 2008). Thus, the assessment of the reliability of temperature data recorded by automatic time-lapse cameras is highly relevant in the context of polar and subpolar research.

To our knowledge, no published study has ever assessed the potential reliability of temperature data recorded by time-lapse cameras by comparing them with air temperature data from a nearby weather station. Dufour-Beausejour et al. (2020) attempted it first in Deception Bay (Nunavik) by comparing air temperature data recorded via time-lapse cameras with temperature data registered at an airfield located about 50 km away from their study site. However, differences of altitude between the instruments, the exposition, and the vegetation surroundings close to the time-lapse camera were not further investigated during the comparisons and data interpretation. Furthermore, parameters that might impact the reliability of temperature data collected by time-lapse cameras such as cloud coverage and downwelling shortwave radiation, were not assessed.

In this study, our aim is to *(i)* identify the main differences in performances between time-lapse cameras and weather stations as temperature measurement tools for studies in remote regions, *(ii)* to document the parameters that are affecting the reliability of temperature data measured by automatic time-lapse cameras. We should note that the cameras used in this study were first set up to document snow-avalanche releases in an ancient glacial valley located in northern Québec so they were in use mainly during winter and spring (Veilleux et al., 2019; Veilleux et al., 2021; Loiseau, 2021; Grenier et al., 2023). Here we took the additional opportunity to test the potential of time-lapse cameras for temperature measurement and to identify the deviations observed at multiple time scales.

2. Study area

Tasiapik Valley (56°33'N, 76°28'W) is a 4.5 km long and 1.5 km wide valley that is located km east of Umiujaq village on the eastern coast of Hudson Bay, Nunavik, Québec (fig. 1A). The valley has a northwest-southeast orientation, and the height of its slopes increases from upstream (around 50 m) to downstream (around 300 m). The relief is characterized as a cuesta, which consists of an anti-conform dip of the front forming the valley slope looking south-eastward, and an asymmetrical shape with a very steep front (near vertical) facing northeast and a gently inclined plateau (about 5° to 10°). There are no wind obstacles such as trees at the summit and on the windward slope (Dionne, 1976; Michaud and Dionne, 1987; Veilleux, 2019).

The Umiujaq region is located within the discontinuous permafrost zone (Allard and Séguin, 1985; Allard et al., 2007). The valley itself is regulated by a microclimate corresponding with the freeze and thaw cycles of Tasiujaq Lake, which warms the air above in the absence of ice (Busseau et al., 2017). The annual mean air temperature remains below 0°C (mainly between −4°C and −6°C). The region receives a yearly average of 645 mm of precipitation, of which about 40% is to snowfall (Ménard et al., 1998; Charron, 2015). The valley floor is discontinuously covered by low shrubs, ericaceous plants, and lichens in the upstream part. Further downstream, closer to Tasiujaq Lake, the vegetation cover changes to a denser forest that includes taller trees.

3. Material and methods

3.1. Automatic time-lapse cameras

Four automatic time-lapse cameras (*Reconyx PC800 Hyperfire time-lapse cameras*) have been strategically placed along Tasiapik Valley's southwestern slope during the summers of 2017 to 2019 to monitor gravity and geomorphic slope process, mainly snow avalanches (Veilleux et al., 2019; Veilleux et al., 2021; Loiseau, 2021; Grenier et al., 2023). One camera is located at the top of the cuesta, near its ridgeline and is essentially used to document the dynamic of a snow cornice during winter as well as possible movements of large chunks of the rock cornice since deep fractures and cracks detached these blocks from the rockface (TAS 1) (fig. 1B-C). The three other cameras are located at the base of the northeast facing slope, near the talus foot, to document snow-avalanche deposits and possible rockfall events (TAS 2, TAS 3, and TAS 4). The cameras have been set to take pictures hourly from 9:00 AM to 5:00 PM during the first year of the investigation. During the second year, the TAS 3 camera was moved to monitor a more downstream snow-avalanche track. The settings of all four cameras were also changed so they would now take pictures from 9:00 AM to 4:00 PM inclusively since we noticed that most of the pictures taken at 5:00 PM were unusable due to early sunsets at Umiujaq latitude (Veilleux et al., 2019). Every camera used in this study is placed in a protective metallic cases. In total, about 25,000 photographs were taken between August 2017 and June 2020. Each photograph was individually inspected to detect the presence of snow-avalanche activity. While inspecting the photographs, we noted for each one the date, the time of day, the temperature recorded by the camera (T_{cam}), in addition to documenting the visible cloud coverage. The cloud coverage was divided in three distinct classes: clear, partly covered, and covered. This data was then used to investigate the relationship between cloud coverage and the precision of cameras at temperature measurement.

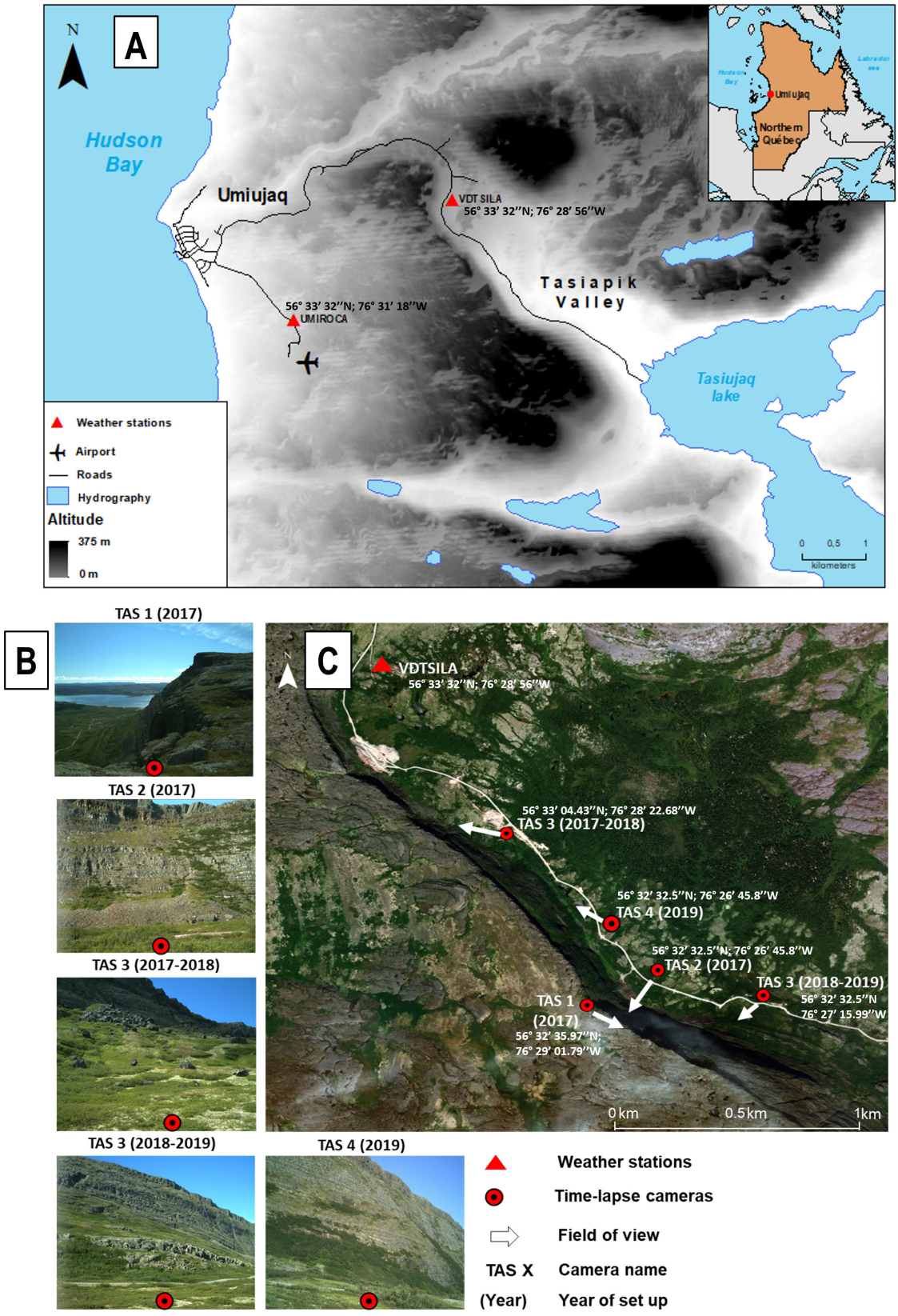

Fig. 1 - Location maps.

A: Location of Tasiapik Valley within the Umiujaq Village area; B: Frame view of each automatic time-lapse camera used in the study; C: Location of automatic time-lapse cameras along Tasiapik Valley SW slope. Data source: Ministère de l'Énergie et des Ressources naturelles (2019), and Ministère des Ressources Naturelles et de la Faune (2019).

Fig. 1 - Cartes de localisation.

A: Localisation de la Vallée Tasiapik dans la région du village d'Umiujaq ; B : Champ de vision de chacun des appareils photographiques utilisés; C : Localisation des appareils photographiques automatisés le long du versant sud-ouest de la Vallée Tasiapik. Source : Ministère de l'Énergie et des Ressources Naturelles (2019), et Ministère des Ressources Naturelles et de la Faune (2019).

3.2. Weather stations

For this study, air temperature data from two automatic weather stations were used. The UMIROCA weather station is located near Umiujaq airfield (approximately 3 km west of the valley), while the VDTSILA is located closer to the cameras, in the upstream part of the valley floor (less than 2 km). The UMIROCA weather station is documenting meteorological conditions in the area since 1997, while the VDTSILA weather station is part of "*Centre d'Etudes Nordiques*" (CEN) climate monitoring SILA network since 2012. The VDTSILA weather station is equipped to measure snow height, liquid precipitations, wind speed and wind orientation at the hourly scale. It is also equipped with a ventilated-heated CNR4 radiometer which provides downwelling shortwave radiation data (CEN, 2020). Data from both weather stations are available for download *via* Nordicana D platform (CEN, 2020). Table 1 details the specification of the temperature probe, time-lapse cameras and CNR4 that are used in this study.

Tab. 1 - Specification of the temperature probe, time-lapse cameras and CNR4 radiometer used in this study.

Tab. 1 - Spécification de la sonde de température, des appareils photographiques à déclenchement automatique et du radiomètre CNR4 utilisés dans cette étude.

Temperature probe	
Manufacturer	Campbell Scientific
Sensor element	- 50° to 100° C
Measurement range	- 50 to 70
Accuracy Worst case	± 0.60° C (-50 to 70° C)
	± 0.25° C (-10 to 70° C)
Steinhart-Hart equation error	≤ 0.03° C (-50 to 70° C)
Time lapse cameras (4)	
Manufacturer	Reconyx
Model	Hyperfire PC 800
CRN4	
Manufacturer	Kipp & Zonen
Response time	< 18 s
Sensitivity	5 to 20 µV w^{-1} m^2
Temperature dependence of sensitivity (- 10° C to + 40° C)	< 4 %
Directional Error	< 20 W m^{-2} (pyranometer); Angles up to 80° with 1,000 $W.m^{-2}$ beam radiation
Operating Temperature Range	- 40° to - 80° C
Spectral Range	305 to 2,800 nm (short wave)
Uncertainty in Daily Total	< 5% (the uncertainty values are for a 95% confidence level)
Spectral Range	4,500 to 42 nm

3.3. Correcting and comparing temperature data

To compare the temperature data registered by the cameras with temperature data registered by the weather stations, we first needed to apply a correction factor to temperature data recorded by the weather stations for them to better represent the actual temperatures at each camera's altitudes. We decided to pair the UMIROCA weather station with the TAS 1 camera since they are both located on the windward slope, just outside the valley limits while the TAS 2, TAS 3 and TAS 4 cameras were paired with the VDTSILA weather station because of their position on the valley floor. Table 2 shows the pairing of weather stations with time-lapse cameras and the respective altitude at which the instruments are located.

To correct the temperature data in alignment with the altitude of each camera, we used the International Standard Atmosphere model (ISA), which states that air cools down one degree every 154 m (–1°C/154 m) (IOS, 1975). To find the altitude-related temperature deviation between a weather station and a camera, we first subtracted the altitude of the weather station from the altitude of the camera (Δ Altitude). Then, we divided ΔAltitude by 154 m to get the temperature deviation between the two locations (T_{alt}) using the following equation:

$$T_{alt} = \frac{(A_{ws} - A_{cam})}{154\ \text{m}} \quad [1]$$

where T_{alt} is the altitude-related temperature deviation between the weather station and the camera; A_{ws} is the altitude of the weather station, and A_{cam} is the altitude of the camera; *(i)* if T_{alt} is positive, it is necessary to add degrees from the temperature originally recorded by the weather stations; *(ii)* If T_{alt} is negative, it is necessary to subtract degrees from the temperature originally recorded by the weather stations.

We then compared the temperature values by subtracting the temperature values recorded on the cameras from those registered by the weather stations post-correction:

$$Deviation = T_{wsc} - T_{cam} \quad [2]$$

where T_{wsc} is the temperature value from the weather station post-correction and T_{cam} is the temperature value recorded by the automatic time-lapse camera. We then interpreted the deviation results as follows: *(i)* when deviation value was negative, the camera over-estimated the temperature, which was corrected from the weather station: ($T_{cam} > T_{wsc}$); *(ii)* when deviation value was positive, the camera underestimated the temperature, which was corrected from the weather station: ($T_{cam} < T_{wsc}$); *(iii)* when deviation value was 0, the camera correctly measured temperature: ($T_{cam} = T_{wsc}$).

4. Results

4.1. Temperature data comparisons

According to the established weather station/camera pairings (tab. 3), we calculated the T_{alt} values, which were then used to correct the temperature recorded by weather stations. This correction enabled the weather stations to better represent the prevailing temperature at each camera's altitude. Table 4 shows the calculated T_{alt} values for each weather station/camera pair. These calculated T_{alt} values were then used as correction factors for altitude-related deviations between the instruments forming a pair.

Once the correction factors (T_{alt}) were applied to the temperatures originally recorded by the weather stations, we could start the comparisons between temperature data registered by time-lapse

Tab. 2: - Pairing of weather stations and automatic time-lapse cameras for temperature measure comparison. The altitude of each instrument is also given.

Tab. 2 - Couplage des stations météorologiques et des appareils photographiques pour les comparaisons. L'altitude pour chaque instrument est aussi donnée.

Weather station	Altitude (m)	Camera	Altitude (m)
UMIROCA	58.7	TAS 1	206
		TAS 2	35
		TAS 3 (2017-2018 position)	75
DTSILA	136	TAS 3 (2018-2019 position)	15
		TAS 4 (2019-2020)	42

cameras and their corresponding weather station. In the context of these comparisons, we first had to select a range around T_{wsc} where T_{cam} values should be considered acceptable. So, we arbitrarily chose to consider a ± 2°C deviation as acceptable in the context of this first exploratory work on the subject as it enables to make a distinction between strictly positive and strictly negative temperature values around freezing point. Furthermore, in the context of snow-avalanche studies such as we are leading, a deviation between, for instance, –22°C and –24°C is quite negligeable during the core of the winter. As a first step, this threshold enabled us to roughly assess the potential of time-lapse cameras at temperature measurement. As shown on Figure 2, the temperature value recorded on every picture taken throughout the study was compared with temperature data from the closest weather station at the same time of the day. Then, we computed the monthly frequency at which T_{cam} was within a range of ± 2°C from T_{wsc}.

During the 2017-2018 study period, the three functioning time-lapse cameras took a total of 8,293 photographs from August 8th, 2017 to June 12th, 2018. The TAS 1 camera captured 2,773, while TAS 2 and the TAS 3 cameras each captured 2,760 photographs. Of the 8,293 total photographs, 5,012 (60%) showed a temperature deviation within ± 2°C of T_{wsc}. The TAS 3 camera was the most accurate, showing 70% of the time deviations within a ± 2°C range of T_{wsc}. It was followed by TAS 1 (55.7%) and TAS 2 (55.3%). We observed that from October to January, most of T_{cam} were very close to T_{wsc}. For instance, in October 2017, the temperatures retrieved from the photographs were 93% of the time within the ± 2°C range. However, we also observed that the number of pictures presenting a temperature deviation greater than ± 2°C drastically increased from February and onward and more specifically during the period from March through June. Overall, April is the month when T_{cam} showed the most pictures with temperature values outside of the ± 2°C range of T_{wsc}. Only 18% of the April photographs showed temperature values within the ± 2°C range of T_{wsc}.

During the 2018-2019 study period, the three cameras took a total 7,299 photographs between August 18th, 2018, and June 19th, 2019 (TAS 1 with 2,376 photographs; TAS 2 with 2,467; TAS 3 with 2,456). The temperatures recorded on 4,705 of them (64%) were now within a ± 2°C range from T_{wsc}. During this period, the TAS 3 camera showed the best results for the second year running, being considered accurate according to our threshold 73% of the time. It was followed by TAS 2 at 61% and TAS 1 at 59%. Again, all three cameras showed a tendency towards more accurate temperatures from October to February, while in March the number of photographs that showed temperature differences greater than ± 2°C from T_{wsc} again increased significantly. The month of December 2018 is when the most accurate camera-recorded temperature values within the ± 2°C range of T_{wsc} were observed. That month, T_{cam} was accurate 89% of the time (659 photographs out of 744), while the month of April was again the month in which the cameras were less accurate at temperature measurement with 29% (212 photographs out of a total of 720) that showed temperature values that were within ± 2°C of T_{wsc}.

During the 2019-2020 study period a fourth Reconyx Hyperfire P800 camera was set up along Tasiapik Valley's southwestern slope during a fieldwork campaign early October 2019. Between September 1st, 2019, and June 30th, 2020, the four cameras took 9,441 photographs. The new TAS 4 camera captured 2,145 of them, while the three other cameras took 2,432 photographs each. Once again, the TAS 3 camera recorded the most photographs with 71% of its recording within ± 2°C of T_{wsc} (1,727 pictures out of 2,432). It was followed by TAS 1 (62%), TAS 2 (59%), and TAS 4 (51%). In total, 5,762 photographs out of 9,441 (61%) showed a temperature value within ± 2°C of T_{wsc}. Data from this year supported the observation of the two previous periods that October was the month when the cameras were most accurate since 89% (842 out of 945 pictures) showed temperature values within ± 2°C from T_{wsc}. In April 2020, the temperature recorded on the photographs were frequently outside the ± 2°C from T_{wsc}. In fact, only 234 out 960 photographs taken by the four cameras (24%) were within ± 2°C of T_{wsc}. These results show that there is a tendency for the cameras to record more accurately the temperature in late autumn and in winter more than in spring.

4.2. Accuracy of time-lapse cameras at temperature measurement

To better examine the precision of time-lapse cameras for temperature measurement, three periods were established (2017-2018, 2018-2019, and 2019-2020) to facilitate year-to-year comparisons and visualisation of tendencies. As T_{cam} were not available year-round, we focused on common time scales. Effectively, the batteries in the cameras did not last a full year, so some data were missing from around mid-June to August, which is the time our team got back in the field to change the batteries and retrieve the photographs from the previous monitoring period. Table 4 details the exact dates over which the comparisons were held.

Tab. 3 - Calculated altitude-related air temperature deviations between weather stations and automatic time-lapse cameras installed within Tasiapik Valley.

Tab. 3 - Variations calculées des différences de températures liées à la différence d'altitude entre les stations météorologiques et les appareils photographiques automatisés dans la Vallée Tasiapik.

Weather station	$A_{ws\ (m)}$	Camera	$A_{cam\ (m)}$	Δ Altitude $_{(m)}$	T_{alt}
UMIROCA	58.7	TAS 1	206	-147.3	-0.95
		TAS 2	35	101	+0.66
		TAS 3 (2017-2018 position)	75	61	+0.40
DTSILA	136	TAS 3 (2018-2019 position)	15	121	+0.79
		TAS 4 (2019-2020)	42	94	+0.61

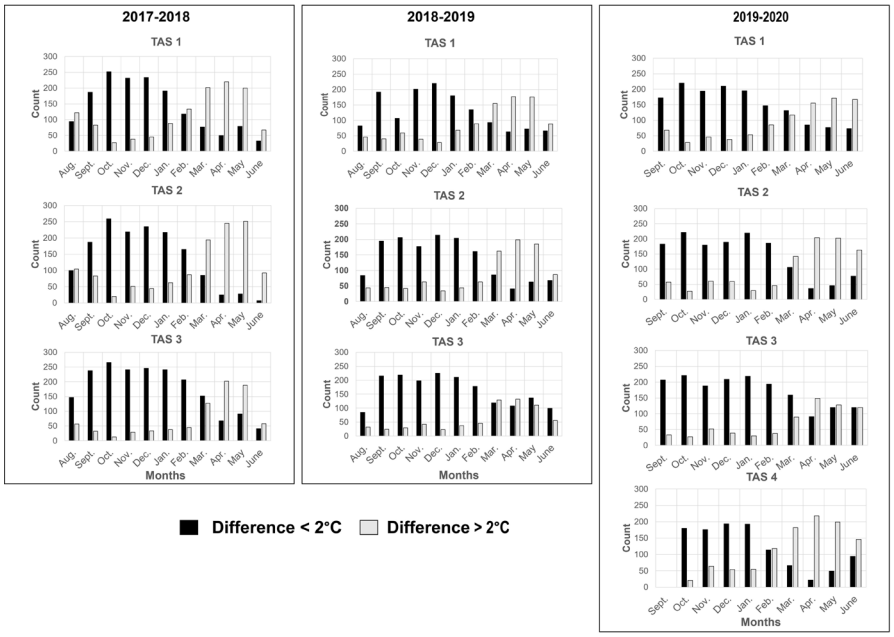

Fig. 2 - Number of pictures taken by time-lapse cameras that showed temperature within ± 2°C of temperature registered by the weather stations.

Fig. 2 - Nombre de photographies prises par les appareils photographiques automatisés qui montraient une différence de température de ± 2°C de celles enregistrées par la station météorologique correspondante.

Tab. 4 - Details of the dates of start and end of the comparison periods for every camera.

Tab. 4 - Détails des dates de début et de fin des périodes de comparaisons pour chacun des appareils photographiques.

	2017-2018		2018-2019		2019-2020	
Camera	**Start**	**End**	**Start**	**End**	**Start**	**End**
TAS 1	2017-08-08	2018-06-12	2018-08-16	2019-06-20	2019-09-01	2020-06-30
TAS 2	2017-08-09	2018-06-11	2018-08-16	2019-06-20	2019-09-01	2020-06-30
TAS 3	2017-08-09	2018-06-11	2018-08-17	2019-06-20	2019-09-01	2020-06-30
TAS 4	-	-	-	-	2019-10-06	2020-06-30

4.2.1. The 2017-2018 period

In 2017-2018, all three cameras globally over-estimated T_{wsc} as shown by the mostly negative mean deviations values presented in Figure 3. From August 8th, 2017, to June 12th, 2018, the TAS 3 camera is the one that performed best at measuring temperature with a yearly mean deviation closest to 0°C at −1.1°C. It was followed respectively by TAS 1 (−2.5°C), and TAS 2 (−2.7°C). Moreover, all three cameras monthly mean deviation curves seem to present a sinusoidal-like shape with mostly negative mean deviations that begins to accentuate in February and March. This accentuation of negative mean deviations is interpreted as the signal that cameras over-estimated even more temperatures during from February and onward. This accentuation of over-estimation signals that cameras might not be reliable for quality temperature data from March to June at our study site.

4.2.2. Monthly scale

T_{cam} were more accurate at measuring temperature in autumn/early winter (*e.g.*, September to January), as the monthly mean deviations remained mostly below ± 2°C with T_{wsc} (Figure 4A). The TAS 1 camera performed the best in October with a monthly mean deviation of −0.1°C, while the TAS 2 camera performed best in January, with a monthly mean deviation of −0.3°C. The negative mean deviation values indicate that both TAS 1 and TAS 2 generally over-estimated temperatures from T_{wsc} in October. For the TAS 3 camera, the most accurate month was September (+0.1°C in average). This positive mean deviation value signals that the TAS 3 camera mostly under-estimated temperature in September, which contrasts with the two other cameras. Positive monthly mean deviation values were also observed for TAS 3 in October, November, December, and January. Between September and February, monthly mean standard deviation values were also quite narrow and remained mainly within ± 2.0°C of T_{wsc} for all three cameras (fig. 4B).

In March, all three cameras started to record less accurate temperature readings, as indicated by the shift of the calculated monthly mean deviations away from 0°C towards the negative side, which signalled greater over-estimations of T_{wsc} by the cameras. The months during which the average deviations were the greatest were March for TAS 1 (−5.4°C), April for TAS 2 (−6.7°C) and May for TAS 3 (−4.3°C). It was also from March to May that the highest standard deviation values were observed, reaching a maximum of ± 4.4°C in March for TAS 1. These negative monthly mean deviations combined with large standard deviations signals that the cameras significantly over estimated temperature from March and onwards.

4.2.3. Hourly scale

The cameras generally performed better earlier in the day (09:00 – 11:00 AM) than during the afternoon (12:00-4:00 PM) (fig. 4C). Both the TAS 1 and TAS 2 cameras showed respective hourly mean

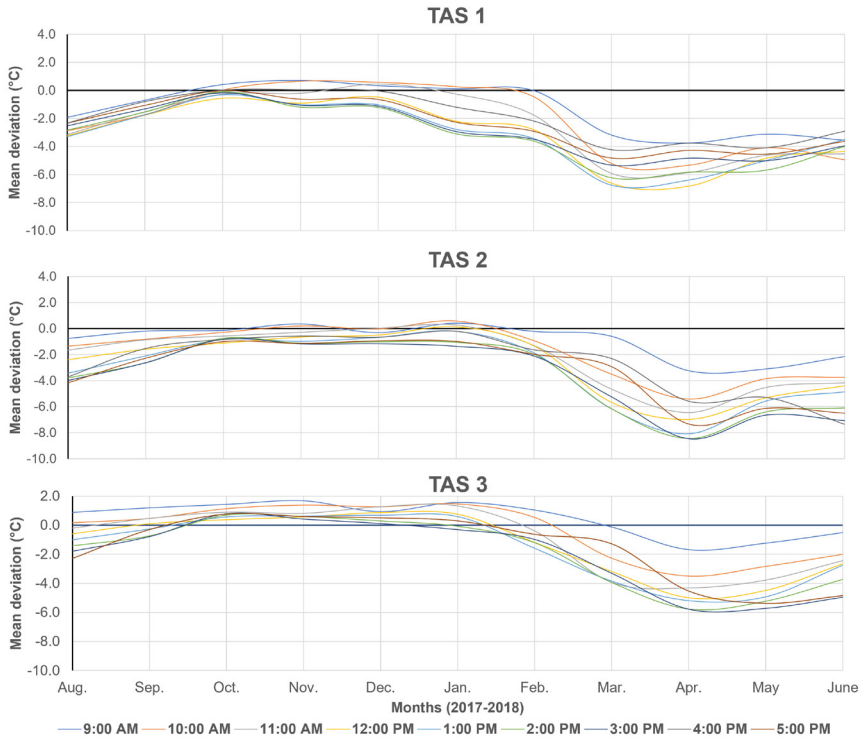

Fig. 3 - Monthly mean deviation for the period 2017-2018, by hour, calculated between the corrected temperature from weather stations and the automatic time-lapse cameras.

A negative mean deviation value indicates that the automatic time-lapse camera overestimated the air temperature value corrected from the weather station.

Fig. 3 - Moyennes mensuelles des écarts de températures pour la période 2017-2018, par heure, entre les températures corrigées des stations météorologiques et les appareils photographiques automatisés.

Une valeur négative de l'écart exprime une surestimation des températures faites par l'appareil photographique automatisé.

deviations of −1.3°C and −0.9°C at 9:00 AM. The TAS 3 camera however generally under-estimated T_{wsc} at 9:00 AM, as shown by a positive mean deviation value (+0.5°C). The TAS 3 camera performed better at 10:00 AM, showing a mean deviation closer to 0°C (−0.4°C). The mean deviation calculated for TAS 3 at 10:00 AM was the lowest that was observed at the hourly scale in 2017-2018, regardless of the camera.

The hours at which the cameras were least accurate were 2:00 PM for TAS 1 (−3.2°C in average) and 3:00 PM for TAS 2 and TAS 3 cameras (respective average deviations of −3.7°C and −2.0°C with the VDTSILA weather station). These were also the times when the mean standard deviation values were the greatest (± 2.8 for TAS 1 at 2:00 PM, ± 2.6 for TAS 2 at 3:00 PM, and ± 2.2 for TAS 3 at 3:00 PM) (fig. 4D).

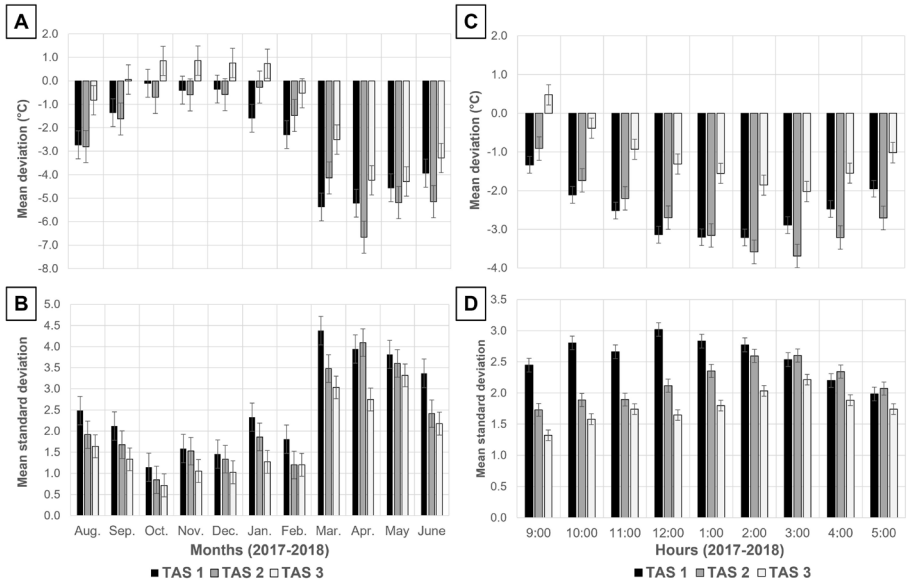

Fig. 4 - Monthly and hourly mean deviation and mean standard deviations of air temperature registered by automatic time-lapse cameras in comparison with air temperature values corrected from the weather stations in 2017-2018.

A: Monthly mean deviations; B: Monthly mean standard deviations; C: Hourly mean deviations; D: Hourly mean standard deviations.

Fig. 4 - Écarts mensuels moyens, horaires moyens, et écarts-types relevés entre les valeurs de températures enregistrées par les appareils photographiques automatisés et les valeurs de températures corrigées des stations météorologiques en 2017-2018.

A : Écarts mensuels moyens ; B : Écarts types mensuels ; C : Écarts horaires moyens ; D : Écart type horaire.

4.3. Synthesis: inter-annual variability and tendencies

To determine whether the mean deviations calculated during the first year were coincidental or not, we repeated the comparisons with temperature data noted on the photographs and data registered by the weather stations in 2018-2019 and in 2019-2020. The results for the periods 2018-2019 and 2019-2020 are further detailed in the supplementary material section of this article. We should reiterate that over summer 2018, the TAS 3 camera was moved further downstream to monitor another avalanche path located within

Tasiapik Valley area.

From year to year, tendencies were observed in the level of precision of time-lapse cameras at temperature measurement and in the times at which the cameras performed best and worse (tab. 5). It highlights that such comparisons are relevant for environmental studies lead in remote regions. With better knowledge of the parameters affecting the temperature measurements produced by automatic time-lapse cameras, a correction model for temperature recorded by such cameras could eventually be proposed. Such a correction model could then serve as a cost-effective alternative for the installation of costly climate monitoring systems for some types of research but also could prevent researchers from using temperature data from weather station that are located very far from the study area.

For instance, the months when the best performances from T_{cam} remained quite early in the study periods (October in 2017-2018; December in 2018-2019; and October again in 2019-2020) whereas the months when the poorest performances were observed late in the periods (March in 2017-2018; April in 2018-2019; and April again in 2019-2020). Regardless of the year, the hour at which TAS 1 was most accurate was always 09:00 AM while the hour at which its performances were the poorest changed from 02:00 PM during the first year to 01:00 PM for the two subsequent years.

The performances observed for the TAS 2 camera showed quite similar patterns than those of TAS 1. The greatest deviations were observed in April, late in the day (2:00 or 3:00 PM) whereas the better performances were observed at 9:00 in December and January. The performances of the TAS 3 camera at temperature measurement were better in September around 10:00 and 11:00 PM.

Tab. 5 - Synthesis of the results and variability in the performances of time-lapse cameras at air temperature measurement.

Tab. 5 - Synthèse des résultats et variabilité des performances des appareils photographiques automatisés observée pour la mesure de températures.

Camera	**TAS 1**			**TAS 2**			**TAS 3**			**TAS 4**		
Period	2017-2018	2018-2019	2019-2020	2017-2018	2018-2019	2019-2020	2017-2018	2018-2019*	2019-2020	2017-2018	2018-2019	2019-2020
Mean deviation (yearly scale, °C)	-2.5	-2.2	-2.0	-2.7	-2.0	-1.9	-1.1	-0.8	-0.7	N/A	N/A	-2.3
Best month	Oct.	Dec.	Oct.	Jan.	Dec.	Dec.	Sep.	Sep.	Sep.	N/A	N/A	Oct.
Worse month	Mar.	Apr.	Apr.	Apr.	Apr.	Apr.	May	Apr.	Apr.	N/A	N/A	Apr.
Best hour	9:00 am	9:00 am	9:00 am	9:00 am	9:00 am	9:00 am	10:00 am	11:00 am	11:00 am	N/A	N/A	9:00 am
Worse hour	2:00 pm	1:00 pm	1:00 pm	3:00 pm	2:00 pm	3:00 pm	3:00 pm	2:00 pm	3:00 pm	N/A	N/A	2:00 pm

Its poorer performances were observed in April and May around 2:00 and 3:00 PM. Because it was installed in October 2019, we could not observe any tendencies nor any interannual variability between the temperature values registered by the TAS 4 camera and by the VDTSILA weather station. However, it showed similar results than the other cameras for the year it was in function. The best performances of TAS 4 at temperature measurement were observed early in the day and the month when it performed best globally was October.

5. Discussion

The results of this study indicate that time-lapse cameras tended to mostly over-estimate temperature from the weather stations from March to June, most often during the afternoon (12:00-3:00 PM), thus regardless of their location within Tasiapik Valley area. According to our field observations and data interpretations, some parameters may affect the reliability of T_{cam}. These parameters include the cloud coverage, the downwelling shortwave radiation, the environmental surroundings of each camera, and the exposure of the cameras.

5.1. Impacts of cloud coverage on the precision of time-lapse cameras

Since portions of the sky were visible on the frame views, we could classify the observed cloud coverage for each photograph. We used three categories: *(i)* clear, *(ii)* partly covered, and *(iii)* covered to describe the relative observed cloud coverage from each photograph's frame view. This data was then used to determine if the observed cloud coverage had any noticeable impact on the accuracy of temperature measurement by cameras.

During the 2017-2018 study period, we observed that the three cameras tended to over-estimate T_{wsc} to a greater degree when the sky was observed as cloud free. Figure 5A shows that all three cameras overestimated to a higher degree temperatures under clear sky conditions than under partly covered or covered sky conditions. The TAS 2 camera was the one that seemed most affected by cloud conditions with an average deviation of –4.9°C with T_{wsc} under cloudless sky conditions.

The same trend was observed during the 2018-2019 study period. The over-estimation of temperatures by the cameras was greater under clear sky conditions than under partly covered, or completely covered sky conditions (fig. 5B). However, the TAS 1 camera was the one that seemed the most affected by the cloud coverage during this period in contrast with TAS 2 during the prior study period. The average deviation between T_{cam} from TAS 1 and T_{wsc} from UMIROCA weather station rose to –4.4°C under clear sky conditions, while the average difference was –1.2°C under covered sky conditions.

In 2019-2020, the TAS 1 camera was again the camera that was most affected by cloud conditions since it over-estimated T_{wsc} by 4.8°C in average under clear sky conditions in comparison with an overestimation of 1°C in average under completely covered sky conditions.

We consider that the differences observed in the performances of T_{cam} at providing accurate T_{wsc} depending on the relative cloud coverage observed from the frame views could be dependant of the types of cloud passing over Tasiapik Valley. Each type of cloud has different effects on incoming solar radiation to Earth. For instance, it was showed in other studies that high thin clouds like cirrus formed in the upper tropospheric regions are more transparent to incoming solar irradiation, but are contributing to the greenhouse

effect and to heating of the Earth by reflecting heat towards the Earth (Platt et al., 1987; Prabhkara et al., 1993; Inoue and Ackerman, 2002). On the other hand, lower and thicker clouds such as cumulus tend to have a cooling effect on Earth by reflecting incoming solar radiation back to space before it reaches Earth (NASA, 1999). A precise characterisation of the clouds present above the Tasiapik Valley study site at the time of each photograph would be an interesting avenue to pursue the research efforts towards a better understanding of the variability in the performances of time-lapse cameras at temperature measurements.

The partial vision of the sky over Tasiapik Valley from the cameras frame view could however be problematic for cloud identification and could result in cloud identification errors. Thus combining the multiple frames we have of the sky over Tasiapik Valley for every time stamp could then provide a better picture and limit the errors concerning the cloud situation over the study to better understand how each type of cloud affects T_{cam}.

Furthermore, results from three two-way ANOVA analyses, showed that the effects of the cloud coverage, the camera that was used, as well as the interaction between the cloud coverage and the camera that was used, are statistically significant (tab. 6). The significant *p-value* for the interaction between the cloud coverage and the camera indicates that the temperature difference between the camera and the weather station depends on the cloud cover and on the camera used itself. Since the cameras are all from the same manufacturer and of the same model (thus should perform the same) it appears that the location of the camera (and more specifically the environmental conditions at each location) might influence its accuracy at temperature measurement. These environmental factors are going to be discussed in a separate section.

The significant *p-values* shown in Table 7 indicate that some of the groups of means are different from others. Then, to determine which group of means are significantly different from which, a post-hoc multiple pairwise comparison was performed using Tukey's Honestly-Significant-Difference test (Tukey, 1949; Montgomery, 2013; Ravichandran and Padmanaban, 2022).

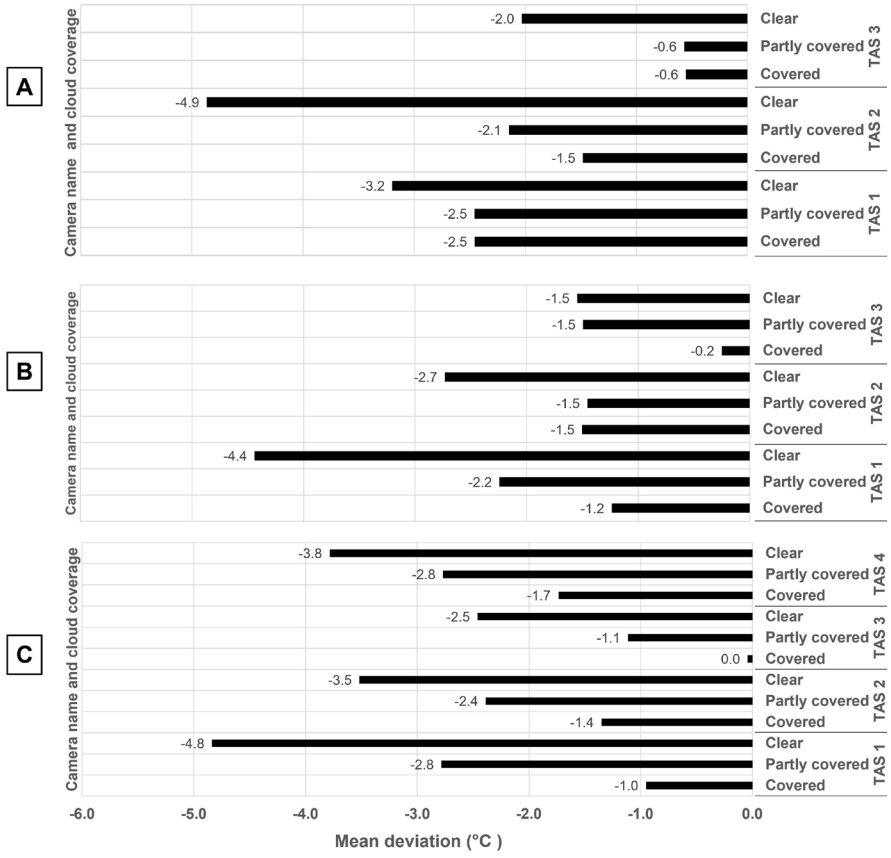

Fig. 5 - Mean deviation (°C) of air temperature computed between the automatic time-lapse cameras and the weather stations according to the cloud coverage.

A: 2017-2018 period; B: 2018-2019 period; C: 2019-2020 period.

Fig. 5 - Écarts de températures moyens (°C) relevés entre les appareils photographiques automatisés et les stations météorologiques en fonction de la couverture nuageuse observée.

A : 2017-2018; B : 2018-2019 ; C : 2019-2020.

Figure 6A shows the results of the multiple pairwise comparisons for the 2017-2018 study period. For the TAS 1 camera, there was a statistically significant difference between the mean deviation under clear sky conditions in comparison with the mean deviation under partly covered sky conditions and under completely covered sky conditions. However, there were no significant difference between the deviations observed under a partly covered sky and a completely covered sky. For the TAS 2 camera, it is shown that the mean of the deviations for all sky conditions significantly differed from each other. For TAS 3, the mean deviation under clear sky condition was again significantly different from the mean deviation under partly covered and covered sky conditions as observed for TAS 1. It is noteworthy that the mean deviation under partly covered sky conditions and under covered sky conditions from TAS 1 did not significantly differ from the mean deviation under clear sky conditions for TAS 3. This result further highlights the importance of the variation in temperature measurement induced by the camera itself and the probable impacts of its surrounding environment.

Figure 6B shows that for TAS 1, during the 2018-2019 study period, all three classes of cloud coverage had significantly different means from each other, the over-estimation being greater under clear sky conditions and less under completely covered sky conditions. For TAS 2, the mean deviation under

Tab. 6 - Two-way ANOVA test, by period for temperature deviations between time-lapse cameras and weather stations by cloud cover, camera, and the interaction between the two.

The symbol « *** » indicates statistical significance.

Tab. 6 - Test ANOVA à deux critères, par période, pour l'écart des températures mesuré observé entre les appareils photographiques et les stations météorologiques selon la couverture nuageuse, l'appareil photographique utilisé et l'interaction des deux.

*Le symbole « *** » indique une significativité statistique.*

Period	Source of deviation	df	Sum of squares	Mean squares	*F-value*	*P-value*
2017-2018	cloudcov	2	4,790	2,394.8	233.38	<2e-16***
	ID_cam	2	4,756	2,377.9	231.72	<2e-16***
	cloudcov: ID_cam	4	1.759	439.6	42.84	<2e-16***
	residuals	7,999	82,079	10.3	-	-
20178-2019	cloudcov	2	5,471	2,735.7	335.17	<2e-16***
	ID_cam	2	2,498	1,248.9	153.01	<2e-16***
	cloudcov: ID_cam	4	1.315	328.8	40.29	<2e-16***
	residuals	7,290	59,503	8.2	-	-
2019-2020	cloudcov	2	8,614	4,307	646.87	<2e-16***
	ID_cam	2	2,643	1,321	198.45	<2e-16***
	cloudcov: ID_cam	4	627	157	23.54	<2e-16***
	residuals	7,287	48,518	7	-	-

clear sky condition was significantly lower than under partly covered and under completely covered sky conditions, signalling again a greater over-estimation under clear sky conditions by this camera. For TAS 3, there was no significant difference between the performances under clear sky conditions and under partly covered sky conditions. Nonetheless, the mean deviations of the two classes significantly differed from the mean deviation observed under completely covered sky conditions. Furthermore, we can again see that the mean deviation under clear sky conditions for TAS 3 did not differ significantly from the mean deviation under a covered sky for TAS 1, and TAS 2, which supports the previous findings that the TAS 3 camera seems to function differently than the two other cameras located in Tasiapik Valley.

Finally, for the 2019-2020 period, Figure 6C shows that for TAS 1, TAS 2, and TAS 3, the mean deviations between the three classes of cloud coverage were all significantly different from each other. The effect of the camera is again visible since the means differ from camera to camera under clear sky conditions.

5.2. Impacts of downwelling short wave radiation on the accuracy of time-lapse cameras at temperature measurement

Since the over-estimation of temperatures by automatic time-lapse cameras in Tasiapik Valley was observed to be greater under clear sky conditions, we decided to test the relationship between daily mean temperature deviations recorded between T_{cam} and T_{wsc} and daily mean downwelling short wave radiation values (see Figure 7A-B (plus Figure 14-15 in supplementary material).

Figure 7A shows that for the 2017-2018 period, temperature values recorded by automatic time-lapse cameras were indeed affected by solar irradiation. Specifically, in August and September, when mean downwelling short wave radiation values were respectively 367 $W.m^{-2}$ and 221 $W.m^{-2}$, time-lapse cameras over-estimated temperature as shown by the negative daily mean deviations values. Over winter, downwelling short wave radiation values dropped lower than 100 $W.m^{-2}$ in average which coincides with the mean deviations getting closer to 0°C. This shows that in winter, time-lapse cameras were quite accurate at temperature measurement. In fact, they rarely indicated temperature values ± 2°C from T_{wsc}. Furthermore, during winter season, we also observe that the daily mean deviations between temperatures values from TAS 3 camera and VDTSILA weather station is often slightly above 0°C, while the daily mean deviations between TAS 2 camera and the VDTSILA weather station is more often below 0°C. It can be interpreted as the signal that the TAS 3 camera tended to under-estimate temperature from VDTSILA whereas TAS 2 overestimated mostly temperatures from VDTSILA.

Starting late February, daily mean downwelling short wave radiation values began to rise back progressively. From then on, cameras all started to over-estimate temperature and their precision at temperature measurement worsened through spring and summer which transcribed by greater negative daily mean deviation values observed (fig. 7A).

Coefficients of correlation between daily mean deviations and solar irradiance showed strong negative correlations (respective *R* values of –0.58 for TAS 1; –0.79 for TAS 2; and –0.82 for TAS 3) meaning that as daily mean downwelling short wave radiation values increased, the cameras over-estimation of temperature increased (greater negative mean deviation values). According to Cohen's classification of coefficients of determination (1988), the TAS 1 camera showed a mid-sized effect correlation (R^2 = 0.34), while both TAS 2 and TAS 3 showed strong effects with daily mean downwelling short wave radiation (R^2 = 0.63 for TAS 2; R^2 = 0.69 for TAS 3) (fig. 7B) suggesting that the deviations observed between temperatures recorded by TAS 2 and TAS 3 cameras and temperatures recorded by VDTSILA weather station can be partly explained by solar irradiance.

When repeating the analysis for the periods 2018-2019 and 2019-2020, very similar results were found. The figures and complete results are detailed in the supplementary material section of the present study. We should note that every time there was a peak in downwelling radiation shortwave values, the overestimation of temperature by cameras also peaked.

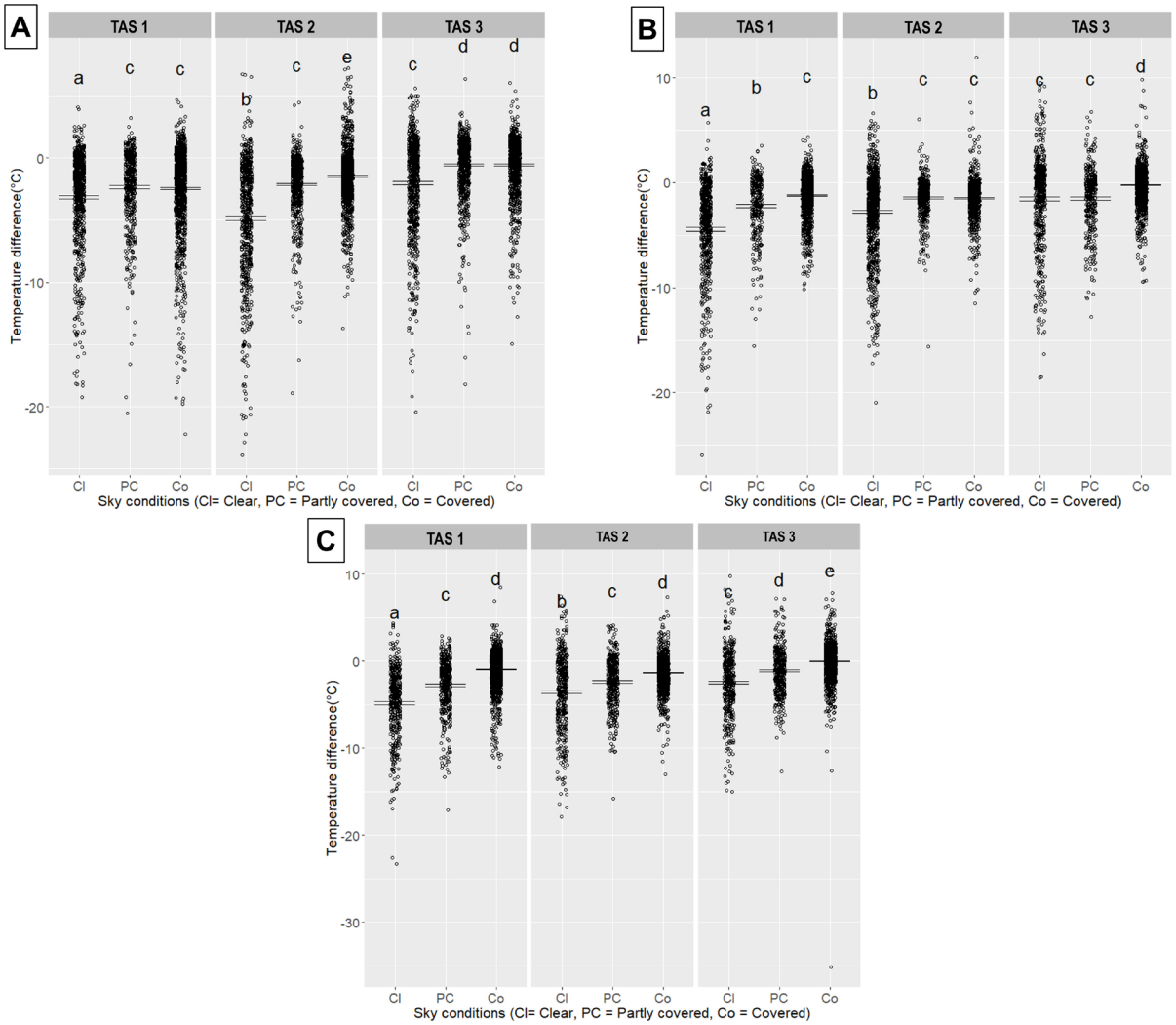

Fig. 6 - Temperature deviations between time-lapse cameras and weather stations in response to the camera that was used and the sky conditions.

Fig. 6 - Écarts de température mesuré observés entre les appareils photographiques et les stations météorologiques en réponse à l'appareil photographique utilisé et la couverture nuageuse.

5.3. Environmental conditions surrounding time-lapse cameras

As shown in the previous section, unlike the three other cameras, the TAS 1 did not seem to be as affected as the three other cameras by solar irradiance. In fact, the TAS 1 camera showed lower coefficients of correlation (*R*) as well as lower coefficients of determination (R^2) with soalr irradiance than the three other time-lapse cameras. Furthermore, it tended to over-estimate temperature earlier in the year and with more intensity than the other cameras monitoring Tasiapik Valley. We believe that these differences in the performances of time-lapse cameras at temperature measurement might be partially explained by their close surroundings. Effectively, the TAS 1 camera is the only one that is positioned at the top of the cuesta relief, right above a thick layer of basalt, no where near any sorts of vegetation. The TAS 2 is located right between a cluster of basalt boulders that likely fell from the top of the cuesta during the regression of the Tyrell Sea and might have been transported further from the slope via sea and/or ice related processes such as ice rafting and ice pushing (Veilleux et al., 2019). The presence of large basalt boulders just below the TAS 2 camera might be an explanation of its poorer performances compared to the TAS 3 camera. On the other hand, the TAS 3 and TAS 4 cameras are located down the slope, near low shrubs zones that are currently in expansion throughout Nunavik (Tremblay, 2010; Tremblay et al., 2012; Ropars and Boudreau, 2012; Provencher-Nolet et al., 2014; Lemay et al., 2018).

The poorer performances of TAS 1 and TAS 2 cameras at temperature measurement might indeed be influenced by the reflective characteristics of the dark layer of basalt over which they are placed. McGreevy (1985) from his experiments on thermal properties of rocks and their possible implications on rock weathering, found that basalt experienced the highest surface temperatures in comparison with sandstone, granite, and chalk because of its low albedo. Based on the principle that darker rocks warm faster than light coloured rocks, Hall et al. (2005) lead an experiment using six bricks painted from black to white with a 20% difference in brightness on each brick which enabled them to conclude that when air temperature is close or slightly above the

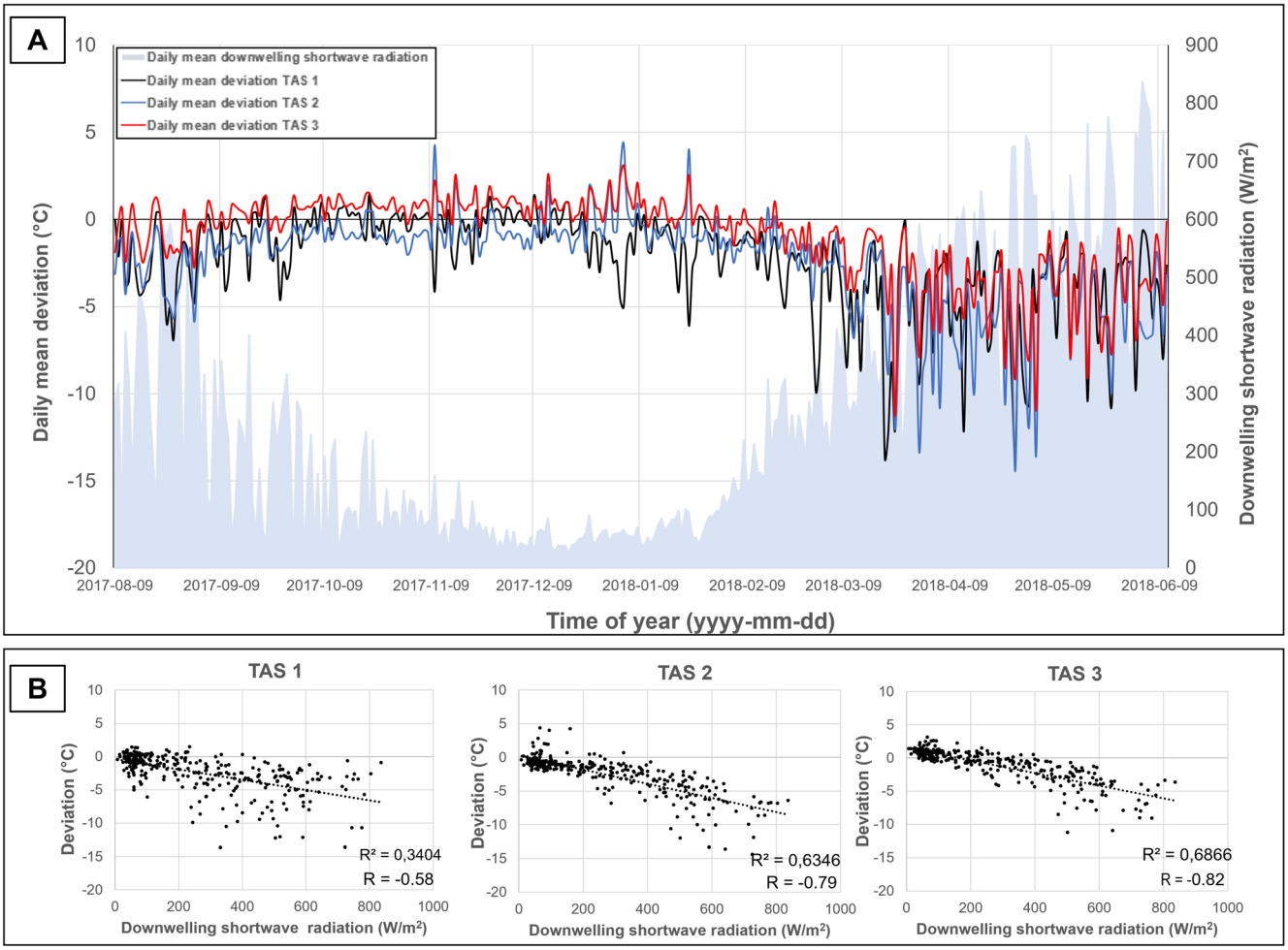

Fig. 7 - Daily mean deviations between air temperature registered on automatic time-lapse cameras and the corrected air temperature values from the weather stations.

A: In relationship with downwelling shortwave radiation from August 9th, 2017, to June 10th, 2018; B: Correlations between daily mean deviations and solar irradiance. Data Source: CEN (2020).

Fig. 7 - Valeurs d'écarts journalières entre les valeurs de températures enregistrées par les appareils photographiques automatisés et les stations météorologiques.

A : En relation avec la radiation solaire incidente journalière moyenne entre le 9 aout 2017 et le 10 juin 2018 ; B : Corrélations entre les écarts moyens journaliers observés et la radiation incidente. Données Source : CEN (2020).

surface temperature of the rock, the theory of the darker rock being hotter held true, but that when air temperature was colder than the rock surface temperature, the darker rock was not the hottest one since it had to release more energy towards the air to warm it by convection and long-wave emissions (Hall et al., 2005). Thus, according to the results of Hall et al. (2005), there is a possibility that TAS 1 and TAS 2 cameras might be affected by the basalt being warmer than the surrounding air. Thus, by means of convection and long-wave emission, the basalt was trying to warm the colder air above, affecting the cameras accuracy at temperature measurement. Unfortunately, we did not have any data for the basalt layer and basalt boulders surface temperature for this study, but it is an avenue that we consider exploring in future research, still with the objective to better understand how we could benefit from the temperature data collected by time-lapse cameras in remote regions where weather stations are not always present.

For the TAS 3 and TAS 4 cameras standing on the valley floor, Ropars and Boudreau (2012) found that shrub densification within the forest-tundra ecotone was significantly greater on sandy terraces than on hilltops but that both types of environments undergo increases in their shrub covers. Since the lower parts of Tasiapik Valley are constituted mostly of marine and littoral sediments (Lajeunesse and Allard, 2003, Lemieux et al., 2016; Fortier et al., 2020) resting on top of fluvio-glacial and glacial deposits (Hillaire-Marcel, 1976), the presence of shrubs on these sandy sediments near the cameras might have helped them register more accurately the temperature and more particularly during early spring. The presence of low shrubs could have contributed to absorb surrounding heat instead of reflecting it towards the cameras. The vegetation could then use this heat for photosynthetic purpose as opposed to the basalt layer at the top of the cuesta which absorbs the solar radiation to warm the surrounding air by releasing sensible heat and emission of longwave radiation. Still, these are hypotheses of why the cameras sitting on the valley floor performed better at temperature measurement than TAS 1 resting at the top of the cuesta and TAS 2 held in place by basalt boulders. These hypotheses need more work but are worth

researching in near future for error modelling purposes. Moreover, it would be interesting in future work to install more captors in the cameras surrounding environment to attempt to better discern and quantify separately the effects of direct solar irradiation and those of the surrounding environment.

5.4. Time-lapse cameras efficiency and problems observed

Throughout this study, we investigated if time-lapse cameras are efficient tools for temperature measurement in remote subarctic areas. Our data interpretation has clearly shown that early in the day and during late autumn and winter, time-lapse cameras are pretty accurate at temperature measurement and that they potentially could be a cost-effective alternative to the use of temperature data collected by further and onerous weather stations and climate monitoring systems. However, we noticed a trend that during the afternoon and especially in spring, the deviations between the temperature recorded by the cameras and the weather stations were sometimes very high.

It is then important to remain very careful if using temperature data registered by these types of time-lapse cameras, and more particularly in spring and in the afternoon. Automatic time-lapse cameras are often used in spring in northern regions because it is a critic period since the frequency of natural hazards such as snow-avalanches (Vogel et al., 2012; Dreier et al., 2016; Gauthier et al., 2017; Laute and Beylich, 2017; Veilleux et al., 2021; Loiseau, 2021), rockfall and landslides due to permafrost thawing (Buteau et al., 2010; Lewkowicz and Way, 2019) and floods (Nilsson et al., 2015; Khalafzai et al., 2021) enhances. Spring is also a crucial time for wildlife (Mizel et al., 2017; Rattenbury et al., 2018; Ram et al., 2019) and vegetation growth (Westergaard-Nielsen et al., 2017; Krab et al., 2018) in arctic and subarctic regions.

Accordingly, one of the main concerns we had with the use of time-lapse cameras as temperature measurement tool was their performances when T_{wsc} were close to 0°C. Effectively we thought that the cameras might register false positive and/or false negative temperature values, expressing false snowmelt or false refreezing, which can be problematic when monitoring snow-avalanche dynamic like we are currently doing in northern Québec (Grenier et al., 2023). As it was shown throughout this study, the cameras performed quite well in winter, when temperature were largely and truly negative, and in late summer/early autumn when temperature were largely and truly positive, but what about when the temperature were close to 0°C? Our data analysis shows that about 6.2% of the total photographs that were taken throughout the study showed false positive values. As shown in Figure 8, these false positive values were mainly observed between the months of March through June. The month of May was overall the most problematic with 22.8% of T_{cam} that showed temperature value above 0°C whilst T_{wsc} was below 0°C. These false positive might be problematic when it is time to evaluate the form of precipitations (snowfall/rainfall).

A further analysis of the false-positive temperature values registered by T_{cam} throughout the study showed that the problem of false positive only occured from March to June. From August to February, the percentage of photographs that showed positive T_{cam} when T_{wsc} was negative remained lower then 5% for all three cameras used (fig. 9). Starting in April, TAS 2 was the camera on

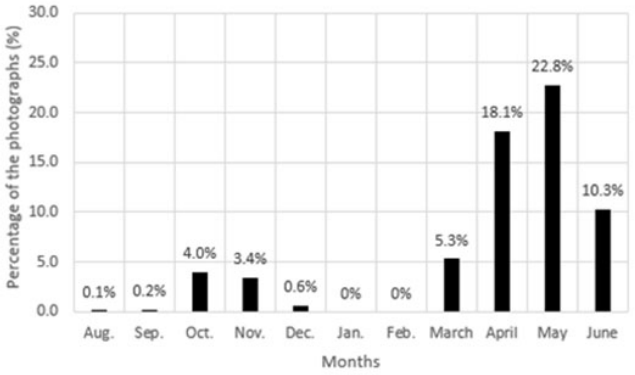

Fig. 8 - Monthly percentage of the photographs taken by automatic time-lapse cameras that showed false-positive temperature values between 2017 and 2020.

Fig. 8 - Pourcentage mensuel des photographies prises par les appareils photographiques automatisés qui montraient des valeurs de températures positives alors que la station météorologique associée montrait une valeur de température négative au même moment entre 2017 et 2020.

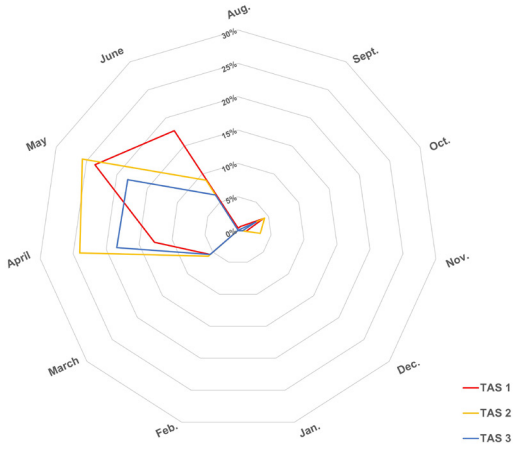

Fig. 9 - Monthly percentage of the photographs taken by automatic time-lapse cameras that showed false positive temperature values between 2017 and 2020, by camera.

Fig. 9 - Pourcentage mensuel des photographies prises par les appareils photographiques automatisés qui montraient des valeurs de températures positives alors que la station météorologique associée montrait une valeur de température négative au même moment entre 2017 et 2020, pour chacun des appareils photographiques.

which the most false-positive temperature values were observed peaking at 26% in May (199 of the 775 pictures registered by TAS 2 in May). Interestingly, Figure 9 also shows that TAS 1 and TAS 2 were the cameras that provided the most pictures with false-positive temperature. Coincidentally, their greater exposition to solar irradiation as well as the basalt found in their close environmental surroundings as described earlier might have played a role in the recordings of warmer temperatures then shown by the weather stations.

At this stage of the study, we were not able to propose a correction model for temperatures recorded by time-lapse cameras because additional parameters such as snow effects and nearby rock temperatures should be held in account. Thus, more work is needed before developing a correction model for temperature recorded *via* automatic time-lapse cameras, but we trust that they could serve as an affective low-cost alternative to the use of data from weather station

systems that can be located as far as 100 km away when working in remote areas in the near future. The advantage of being located *in-situ* is not negligible when working in everchanging northern environments. Throughout the entire study, it was highlighted that a total of 62% of T_{cam} data was relevant, as the gap with real air temperature was less than ± 2°C, further expressing the potential of such devices in remote area research.

6. Conclusion

This study enabled the assessment of the potential of automatic time-lapse cameras at temperature measurement by comparing data retrieved from photographs (T_{cam}) with data from two nearby weather stations located in a 5 km radius (T_{wsc}) in Tasiapik Valley near Umiuaq, in Nunavik. Our results indicate that cameras performed quite well at temperature measurement from late August to the onset of February; the best performances (closest to 0°C deviations between T_{cam} and T_{wsc} occurred early in the study periods (October to December). On the other hand, the weaker performances occurred late winter and spring (March and April), with severer flaws around the freezing point; these are clearly highlighted in this paper. Whenever in the year, time-lapse cameras were most accurate in the morning (at 09:00 AM and 10:00 AM), while in the afternoon (from 12:00 PM to 3:00 PM), they tended to over-estimate temperatures given by the weather stations. The correlation of our data (daily mean deviations of temperature observed between T_{cam} and T_{wsc}) with 1) cloud coverage noted from each camera's frame view and 2) daily mean downwelling shortwave radiation indicate that the over-estimation of temperatures by automatic time-lapse cameras in Tasiapik Valley was greater under clear sky conditions and when mean downwelling shortwave radiation values were high, from February to June. Our work also highlights the potential of time-lapse cameras, which are worth a use to document, in addition to temperature values, the cloud coverage over regular periods of time which can be very important in the context of Earth's radiative budget calculations and in climatological research purposes.

Acknowledgements

We gratefully acknowledge the *Centre d'Etudes Nordiques* (CEN), a strategic cluster funded by the *Fonds québécois de recherche Nature et Technologie*, for access to its research infrastructure for professional and logistical support. Special thanks are extended to the community of Umiujaq for its ongoing support. The authors would also like to thank Samuel Veilleux, Denis Sarrazin, Carl Barrette, Félix Faucher, Julien Lebrun, and Þorsteinn Sæmundsson for their valuable help in the field, and the reviewers for their useful comments on the first versions of the manuscript.

Funding for this project was provided by the Natural Sciences and Engineering Research Council of Canada (NSERC), IPEV #1148 DeSiGN, LabEx DRIIHM (French program "*Investissements d'Avenir*" ANR-11-LABX-0010) and OHMi Nunavik.

References

Abermann J., Eckerstorfer M., Malnes E., Hansen B. U. (2019) - A large wet snow avalanche cycle in West Greenland quantified using remote sensing and in situ observations. Natural Hazards, 97 (2), 517–534.
DOI : 10.1007/s11069-019-03655-8

Allard M., Seguin M.K. (1985) — La déglaciation d'une partie du versant hudsonien québécois : bassins des rivières Nastapoca, Sheldrake et à l'Eau Claire. Géographie physique et Quaternaire, 39 (1), 13–24.
DOI : 10.7202/032581ar

Allard M., Calmels F., Fortier D., Laurent C., L'Hérault E., Vinet F. (2007) — Cartographie des conditions de pergélisol dans les communautés du Nunavik en vue de l'adaptation au réchauffement climatique. Centre d'études nordiques, 49 p.

Busseau B.-C., Royer A., Roy A., Langlois A., Dominé F. (2017) - Analysis of snow-vegetation interactions in the low Arctic-Subarctic transition zone (northeastern Canada). Physical Geography, 38 (2), 159–75.
DOI : 10.1080/02723646.2017.1283477

Buteau S., Fortier R., Allard M. (2010) — Permafrost Weakening as a Potential Impact of Climatic Warming. Journal of Cold Regions Engineering, 24 (1), 1–18.
DOI : 10.1061/(ASCE)0887-381X(2010)24:1(1)

CEN (2020) - Climate station data from the Umiujaq region in Nunavik, Quebec, Canada, v. 1.7 (1997-2019). Nordicana D9. website link: http://www.cen.ulaval.ca/nordicanad/dpage.aspx?doi=45120SL-067305A53E914AF0
DOI : 10.5885/45120SL-067305A53E914AF0

Charron I. (2015) - Élaboration du portrait climatique régional du Nunavik. Ouranos report, Montréal, 100 p.

Cohen J. (1988) - Statistical power analysis for the behavioral sciences. Lawrence Erlbaum Associates, New York, 579 p.

Decaulne A., Bhiry N., Lebrun J., Veilleux S., Sarrazin D. (2018) - Geomorphic evidence of Holocene slope dynamics on the Canadian shield - a study from Lac à l'Eau-Claire, western Nunavik. Écoscience, 25 (4), 343–57.
DOI : 10.1080/11956860.2018.1431376

Dionne J.-C. (1976) - Les grandes cuestas de la mer d'Hudson. GÉOS - Energie, Mines et Ressources Canada, 5 (1), 18–20.

Dreier L., Harvey S., van Herwijnen A., Mitterer C. (2016) - Relating meteorological parameters to glide-snow avalanche activity. Cold Regions Science and Technology, 128, 57–68.
DOI : 10.1016/j.coldregions.2016.05.003

Dufour-Beauséjour S., Wendleder A., Gauthier Y., Bernier M., Poulin J., Gilbert V., Tuniq, J., Rouleau A., Roth A. (2020) - Seasonal timeline for snow-covered sea ice processes in Nunavik's Deception Bay from TerraSAR-X and time-lapse photography. The Cryosphere, 14, 1595–1609.
DOI : 10.5194/tc-2019-199

Eckerstorfer M., Bühler Y., Frauenfelder R., Malnes E. (2016) - Remote sensing of snow avalanches: Recent advances, potential, and limitations. Cold Regions Science and Technology, 121, 126–40.
DOI : 10.1016/j.coldregions.2015.11.001

Eckerstorfer M., Christiansen H. H., Rubensdotter L., Vogel S. (2013a) - The geomorphological effect of cornice fall avalanches in the Longyeardalen valley, Svalbard. The Cryosphere, 7 (5), 1361–1374.
DOI : 10.5194/tc-7-1361-2013

Eckerstorfer M., Christiansen H.H., Vogel S., Rubensdotter

L. (2013b) - Snow cornice dynamics as a control on plateau edge erosion in central Svalbard. Earth Surface Processes and Landforms, 38 (5), 466–476.
DOI : 10.1002/esp.3292

Fortier R., Banville D.R., Lévesque R., Lemieux J.M., Molson J., Therrien R., Ouellet M. (2020) - Development of a three-dimensional geological model, based on Quaternary chronology, geological mapping, and geophysical investigation, of a watershed in the discontinuous permafrost zone near Umiujaq (Nunavik, Canada). Hydrogeology Journal, 28 (3), 813–832.
DOI : 10.1007/s10040-020-02113-1

Gauthier F., Germain D., Hétu, B. (2017) - Logistic model as a forecasting tool for snow avalanches in a cold maritime climate: northern Gaspésie, Québec, Canada. Natural Hazards, 89 (1), 201–232.
DOI : 10.1007/s11069-017-2959-3

Gauthier F., Hétu B., Bergeron N. (2012) - Analyses statistiques des conditions climatiques propices aux chutes de blocs de glace dans les corridors routiers du nord de la Gaspésie, Québec, Canada. Canadian Geotechnical Journal, 49 (12), 1408–1426.
DOI : 10.1139/cgj-2011-0394.

Grenier J., Bhiry N., Decaulne A. (2023) - Meteorological conditions and snow-avalanche occurrence over three snow seasons (2017–2020) in Tasiapik Valley, Umiujaq, Nunavik. Arctic, Antarctic, and Alpine Research, 2023, 55 (1), 2194492.
DOI : 10.1080/15230430.2023.2194492

Hall K., Staffan Lindgren B., Jackson P. (2005) - Rock albedo and monitoring of thermal conditions in respect of weathering: some expected and some unexpected results. Earth Surface Processes and Landforms, 30 (1), 801–811.
DOI : 10.1002/esp.1189

Hillaire-Marcel C. (1976) - La déglaciation et le relèvement isostatique sur la côte est de la baie d'Hudson. Cahiers de Géographie du Québec, 20 (50), 185–220.
DOI : 10.7202/021319ar

Inoue T., Ackerman S.A. (2002) - Radiative Effects of Various Cloud Types as Classified by the Split Window Technique over the Eastern Sub-tropical Pacific Derived from Collocated ERBE and AVHRR Data. Journal of the Meteorological Society of Japan, 80 (6), 1383–1394.
DOI : 10.2151/jmsj.80.1383

International Organization for Standardization (1975) - Standard Atmosphere, ISO 2533.

Khalafzai M.-A.K., McGee T.K., Parlee B. (2021) - Spring flooding and recurring evacuations of Kashechewan First Nation, northern Ontario, Canada. International Journal of Disaster Risk Reduction, 63, 102443.
DOI : 10.1016/j.ijdrr.2021.102443

Krab E.J., Roennefarth J., Becher M., Blume-Werry G., Keuper F., Klaminder J., Kreyling J., Makoto K., Milbau A., Dorrepaal E., Lau, J. (2018) - Winter warming effects on tundra shrub performance are species-specific and dependent on spring conditions. Journal of Ecology, 106 (2), 599–612.
DOI : 10.1111/1365-2745.12872

Lajeunesse P., Allard M. (2003) - The Nastapoka drift belt, eastern Hudson Bay: Implications of a stillstand of the Quebec-Labrador ice margin in the Tyrrell Sea at 8 ka BP. Canadian Journal of Earth Sciences, 40 (1), 65–76.
DOI : 10.1139/e02-085

Laute K., Beylich A.A. (2014) - Morphometric and meteorological controls on recent snow avalanche distribution and activity at hillslopes in steep mountain valleys in western Norway. Geomorphology, 218, 16–34.
DOI : 10.1016/j.geomorph.2013.06.006

Laute K., Beylich A.A. (2018) - Potential effects of climate change on future snow avalanche activity in western Norway deduced from meteorological data. Geografiska Annaler (Series A - Physical Geography), 100 (2), 163–184.
DOI : 10.1080/04353676.2018.1425622

Lemay M.-A., Provencher-Nolet L., Bernier M., Lévesque E., Boudreau S. (2018) - Spatially explicit modeling and prediction of shrub cover increase near Umiujaq, Nunavik. Ecological Monographs, 33 (3), 385–407.
DOI : 10.1002/ecm.1296

Lemieux J.-M., Fortier R., Talbot-Poulin M.-C., Molson J., Therrien R., Ouellet M., Murray R. (2016) — Groundwater occurrence in cold environments: examples from Nunavik, Canada. Hydrogeology Journal, 24 (6), 1497–1513.
DOI : 10.1007/s10040-016-1411-1

Lewkowicz A. G., Way R.G. (2019) - Extremes of summer climate trigger thousands of thermokarst landslides in a High Arctic environment. Nature Communications, 10 (1), 1329.
DOI : 10.1038/s41467-019-09314-7

Loiseau R. (2021) - Étude des avalanches à Umiujaq (Nunavik, Canada) : Persistance des dépôts et distances de parcours. Mémoire de Master, Université de Grenoble, 35 p.

McGreevy J.P. (1985) - Thermal properties as controls on rock surface temperature maxima, and possible implications for rock weathering. Earth Surface Processes and Landforms, 10, 125–136.
DOI : 10.1002/esp.3290100205

Ménard É., Allard M., Michaud Y. (1998) - Monitoring of ground surface temperatures in various biophysical micro-environments near Umiujaq, eastern Hudson Bay, Canada. In Proceedings of the 7th International Conference on Permafrost. Yellowknife, Canada, 723–729.

Michaud Y., Dionne J.-C. (1987) - Altération des substrats rocheux et rôle du soulèvement gélival dans la formation des champs de blocaille, en Hudsonie. Géographie Physique et Quaternaire, 41 (1), 7–18.
DOI : 10,7202/032661ar

Mizel J.D., Schmidt J.H., McIntyre C.L., Lindberg M.S. (2017) - Subarctic-breeding passerines exhibit phenological resilience to extreme spring conditions. Ecosphere, 8 (2), e01680.
DOI : 10.1002/ecs2.1680

Montgomery D.C. (2013) - Design and Analysis of Experiments. Eighth Edit. Wiley, 688 p.

Munroe J.S. (2018) - Monitoring snowbank processes and cornice fall avalanches with time-lapse photography. Cold Regions Science and Technology, 154, 32–41.
DOI : 10.1016/j.coldregions.2018.06.006

National Aeronautics and Space Administration - NASA (1999) - Clouds and the Energy Cycle. The Earth Science Enterprise Series, NASA Facts 207, 6 p.

Nilsson C., Polvi L. E., Lind L. (2015) - Extreme events in streams

and rivers in arctic and subarctic regions in an uncertain future. Freshwater Biology, 60 (12), 2535–2546.
DOI : 10.1111/fwb.12477

Peitzsch E. H., Hendrikx J., Fagre D. B., Reardon B. (2012) — Examining spring wet slab and glide avalanche occurrence along the Going-to-the-Sun Road corridor, Glacier National Park, Montana, USA. Cold Regions Science and Technology, 78, 73–81.
DOI : 10.1016/j.coldregions.2012.01.012

Pigeon K.E., Jiskoot H. (2008) - Meteorological Controls on Snowpack Formation and Dynamics in the Southern Canadian Rocky Mountains. Arctic, Antarctic, and Alpine Research, 40 (4), 716–730.
DOI : 10.1657/1523-0430(07-054)[pigeon]2.0.Co;2

Platt C.M.R., Scott J.C., Dilley A.C. (1987) - Remote sounding of high clouds PartVI: optical properties of midlatitude and tropical cirrus. Journal of Atmospheric Science, 44 (4), 729–747.
DOI : 10.1175/1520-0469(1987)044<0729:RSOHCP>2.0.CO;2

Prabhakara C., Kratz D.P., Yoo J.-M., Dalu G., Vernekar A. (1987) - Optically thin cirrus clouds: radiative impact on the warm pool. Journal of Quantitative Spectroscopy and Radiative Transfer, 49 (5), 467–483.
DOI: 10.1016/0022-4073(93)90061-L

Provencher-Nolet L., Bernier M., Lévesque E. (2014) - Quantification des changements récents à l'écotone forêt-toundra à partir de l'analyse numérique de photographies aériennes. Écoscience, 21 (3-4), 419–433.

Ram D., Ingemar Nyholm N.E., Arlt D., Lindstrom A. (2019) - Small changes in timing of breeding among subarctic passerines over a 32-year period. IBIS - International Journal of Avian Science, 161 (4), 730–743.
DOI : 10.1111/ibi.12682

Rattenbury K.L., Schmidt J.H., Swanson D.K., Borg B.L., Mangiapane B.A., Sousanes P.J. (2018) - Delayed spring onset drives declines in abundance and recruitment in a mountain ungulate. Ecosphere, 9 (11), e02512.
DOI : 10.1002/ecs2.2513

Ravichandran C., Padmanaban G. (2022) - A numerical simulation-based method to predict floor wise distribution of cooling loads in Indian residences using Tukey honest significant difference test. Advances in Building Energy Research, 17 (1), 1–29.
DOI : 10.1080/17512549.2022.2129449

Ropars P, Boudreau S. (2012) - Shrub expansion at the forest-tundra ecotone: spatial heterogeneity linked to local topography. Environmental Research Letters, 7, 015501.
DOI : 0.1088/1748-9326/7/1/015501

Tremblay B. (2010) - Augmentation récente du couvert ligneux érigé dans les environs de Kangiqsualujjuaq (Nunavik, Québec). MSc Thesis, Université du Québec à Trois-Rivières, Québec, Canada, 63 p.

Tremblay B., Lévesque E.**, Boudreau S. (2012)** - Recent expansion of erect shrubs in the Low Arctic: evidence from Eastern Nunavik. Environmental Research Letters, 7, 035501.
DOI : 10.1088/1748-9326/7/3/035501

Tukey J. (1949) - Comparing Individual Means in the Analysis of Variance. Biometrics, 5 (2), 99–114.
DOI : 10.2307/3001913

van Herwijnen A., Fierz C. (2014) - Monitoring snow cornice development using timelapse photography. In Proceedings of the International Snow Science Workshop, Grenoble – Chamonix Mont Blanc, 865–869.

van Herwijnen A., Berthod N., Simenhois R., Mitterer C. (2013) - Using time-lapse photography in avalanche research. In Proceedings of the International Snow Science Workshop, Grenoble – Chamonix Mont Blanc, 950–954.

Veilleux S. (2019) - Processus gravitaires dans la vallée Tasiapik (Nunavik) : témoins géomorphologiques de la dynamique de versant récente et passée. MSc Thesis, Université Laval, Québec, Canada, 94 p.

Veilleux S., Decaulne A., Bhiry N. (2021) - Snow-cornice and snow-avalanche monitoring using automatic time-lapse cameras in Tasiapik Valley, Nunavik (Québec) during the winter of 2017-18. Arctic Science, 7 (4), 798–812.
DOI : 10.1139/as-2020-0013

Vogel S., Eckerstorfer M., Christiansen H.H. (2012) - Cornice dynamics and meteorological control at Gruvefjellet, Central Svalbard. The Cryosphere, 6 (1), 157–171.
DOI : 10.5194/tc-6-157-2012

Westergaard-Nielsen A., Lund M., Pedersen S.H., Schmidt N.M., Klosterman S., Abermann J., Hansen B.U. (2017) - Transitions in high-Arctic vegetation growth patterns and ecosystem productivity tracked with automated cameras from 2000 to 2013. Ambio, 46, 39–52.
DOI : 10.1007/s13280-016-0864-8

Version abrégée en français

Les appareils photographiques à déclenchement automatiques, ou caméras automatiques, sont largement utilisés pour observer les processus liés à la neige et à la glace dans les régions froides, offrant des avantages tels que l'accessibilité à des terrains éloignés et la collecte continue de données sans perturber l'environnement. Équipées de capteurs thermiques, elles fournissent non seulement des informations visuelles mais également des données de température. Cependant, la fiabilité de la donnée de température ainsi enregistrée mérite d'être analysée. Les chercheurs s'appuient souvent sur des stations météorologiques éloignées pour obtenir des données météorologiques précises, ce qui pose des défis dans les régions reculées où les conditions d'isolement ne le permettent pas. Malgré leur utilisation répandue, la fiabilité des données de température provenant de ces appareils photographiques par rapport aux stations météorologiques reste largement inexplorée. Cette étude vise à identifier les différences de performance et à les quantifier, et à documenter les facteurs influençant la fiabilité des données de température proposées, pour évaluer l'efficacité des caméras automatiques dans la mesure de la température en comparant les données des photographies (T_{cam}) avec celles de stations météorologiques voisines (T_{wsc}).

L'étude prend appui dans la vallée de Tasiapik, proche du village d'Umiujaq, au Nunavik (fig. 1). Son orientation est nord-ouest/sud-est et les pentes sont croissantes de l'amont (environ 50 m de dénivelé) vers l'aval (environ 300 m). La région, dans la zone de pergélisol discontinu, est influencée par un microclimat lié aux cycles de gel et de dégel du lac Tasiujaq, maintenant une température annuelle moyenne inférieure à 0°C, avec 645 mm de précipitations annuelles,

dont environ 40 % en neige.

Quatre appareils photographiques à déclenchement automatique Reconyx (tab. 1) ont été placés le long de la pente sud-ouest de la vallée (fig. 1). Environ 25 000 photos ont été prises entre 2017 et 2020, analysées pour détecter les activités d'avalanche et étudier leur corrélation avec la couverture nuageuse et la température enregistrée. Les données de température proviennent de deux stations météorologiques automatiques, UMIROCA et VDTSILA (tab. 2), situées près de la vallée de Tasiapik. Pour comparer les données de température enregistrées par les caméras avec celles des stations météorologiques, nous avons appliqué un facteur de correction pour tenir compte des altitudes différentes (tab. 3). Nous avons utilisé le modèle de l'Atmosphère Standard International pour calculer les écarts de température liés à l'altitude (T_{alt}) (tab. 3). Nous avons ensuite évalué la précision des caméras en considérant une déviation arbitraire de ± 2°C comme acceptable. La majorité des photos prises pendant les études montraient des températures proches de celles des stations météo, mais des écarts significatifs ont été observés au printemps. Au cours des périodes d'étude, les caméras ont montré des précisions variables (fig. 2), avec une tendance à être plus précises d'octobre à février. Cependant, à partir de mars, les écarts de température ont augmenté, avec une précision moins fiable en avril. Les résultats indiquent une meilleure précision des caméras en automne et en hiver par rapport au printemps.

Les comparaisons entre les données de température des caméras (tab. 4) et celles des stations météorologiques pour les périodes 2018-2019 et 2019-2020 ont été répétées pour déterminer si les déviations moyennes calculées la première année étaient fortuites ou non. Les résultats détaillés pour ces périodes sont disponibles dans la section supplémentaire de cet article. Des tendances annuelles ont été observées dans la précision des appareils photographiques à déclenchement automatique pour la mesure de la température (fig. 3) ainsi que dans les périodes, mensuelle et horaire où ils ont le mieux et le moins bien fonctionné (fig. 4, tab. 5). Ces comparaisons s'avèrent pertinentes pour les études environnementales menées dans des régions éloignées. Une meilleure compréhension des paramètres affectant la mesure de la température par ces appareils pourrait conduire à un modèle de correction pour les données de température enregistrées par ces dernières. Ce modèle de correction pourrait être une alternative économique à l'installation de systèmes de surveillance climatique coûteux pour certains types de recherches et éviterait également aux chercheurs d'utiliser des données de température de stations météorologiques situées très loin de la zone d'étude. Par exemple, les performances optimales de T_{cam} sont restées assez constantes au début des périodes hivernales, tandis que les performances les plus faibles ont été observées plutôt au printemps. Quelle que soit l'année, l'heure à laquelle TAS 1 était le plus précis était toujours 09:00 AM, tandis que celle où ses performances étaient les plus faibles a changé. Les performances de TAS 2 ont montré des schémas assez similaires à celles de TAS 1, tandis que les performances de TAS 3 étaient meilleures en septembre et moins bonnes en avril et mai. TAS 4 a montré des résultats similaires aux autres caméras pour l'année où il était en fonction, avec de meilleures performances tôt le matin et une meilleure performance globale en octobre.

Cette étude révèle que les appareils photographiques à déclenchement automatique ont tendance à surestimer la température par rapport aux stations météorologiques de mars à juin, surtout l'après-midi (12h-15h), quel que soit leur emplacement dans la vallée de Tasiapik. Selon nos observations sur le terrain et nos interprétations des données, certains paramètres peuvent influencer la fiabilité des capteurs, notamment la couverture nuageuse (fig. 5, tab. 6), le rayonnement solaire incident, l'environnement entourant chaque caméra et leur exposition. L'impact de la couverture nuageuse a été examiné, montrant une tendance à surestimer la température par temps clair, avec des différences entre les caméras (fig. 6). De plus, une corrélation a été observée entre le rayonnement solaire incident et les écarts de température constatés entre T_{cam} et T_{wsc}, avec des valeurs plus élevées de rayonnement solaire associées à une plus grande surestimation de la température par les caméras (fig. 7). Les conditions environnementales autour des caméras, comme la présence de basalte foncé et de végétation, ont également influencé leurs performances. Les caméras situées près du basalte ont tendance à surestimer la température, tandis que celles près de la végétation ont montré une meilleure précision. Malgré ces défis, les appareils photographiques à déclenchement automatique se sont avérés être des outils efficaces pour la mesure de la température, en particulier tôt le matin et en hiver. Cependant, il est essentiel de rester prudent lors de l'utilisation des données de température enregistrées par ces caméras, surtout au printemps et l'après-midi. Des recherches supplémentaires sont nécessaires pour élaborer un modèle de correction prenant en compte ces facteurs environnementaux afin d'optimiser l'utilisation des caméras à laps de temps dans les régions éloignées. Environ 62% des données de température sont jugées pertinentes, avec un écart de moins de ± 2°C par rapport à la température réelle, ce qui souligne le potentiel de ces appareils pour la recherche en zones reculées (jusque 100% au cœur de l'hiver, 82% en avril) (fig. 8, 9).

Au final, cette étude a évalué l'efficacité des caméras automatiques dans la mesure de la température en comparant les données des photographies avec celles de stations météorologiques voisines dans la vallée de Tasiapik, au Nunavik. Les caméras ont bien fonctionné de fin août à début février, avec les meilleures performances entre octobre et décembre, mais ont montré des performances moindres en fin d'hiver et au printemps. Elles étaient plus précises le matin et tendaient à surestimer les températures l'après-midi. Nos résultats suggèrent également que la surestimation des températures par les caméras était plus prononcée sous un ciel dégagé et lorsque le rayonnement solaire est élevé, de février à juin. On le voit, la fiabilité des températures obtenues via les caméras automatiques n'est pas optimale; cependant, ce travail met en évidence le potentiel des appareils photographiques à déclenchement automatique pour pallier au manque de données de températures dans les zones isolées, très largement inexploitée jusqu'à présent, et pour documenter la couverture nuageuse, ce qui est crucial pour les calculs du bilan radiatif de la Terre et pour la recherche climatologique.

Supplementary material

1. The 2018-2019 period

Over summer 2018, the TAS 3 camera was moved further downstream. During this period, results were roughly similar than those from 2017-2018, as shown by the sinusoidal-like shape of the mean deviations curves presented in Figure 10. We observed mostly negative average deviations, which indicates that

the cameras also over-estimated temperature between August 18th, 2018, and June 19th, 2019. Moreover, the yearly mean deviations of all three cameras were closer to 0°C in comparison with the first year. Even though it had been repositioned within the valley area, the TAS 3 camera was again the camera that performed best overall, with a mean deviation of –0.8°C In contrast with the first year, the TAS 2 camera was the second most accurate camera (–2.0°C), while the TAS 1 camera followed closely (–2.2°C).

1.1. Monthly scale

At the monthly scale, T_{cam} were more accurate from September to February alike on the previous year (fig. 11A). However, unlike on the first year, both TAS 1 and TAS 2 cameras performed best in December rather than October, with respective mean deviations of –0.3°C and –0.5°C. The TAS 3 camera performed best in September and it again mostly under-estimated tem peratures from September to January despite its relocation. Standard deviation values were also at their lowest between August and February for all three cameras, remaining constantly lower than ± 2.5°C (fig. 11B).

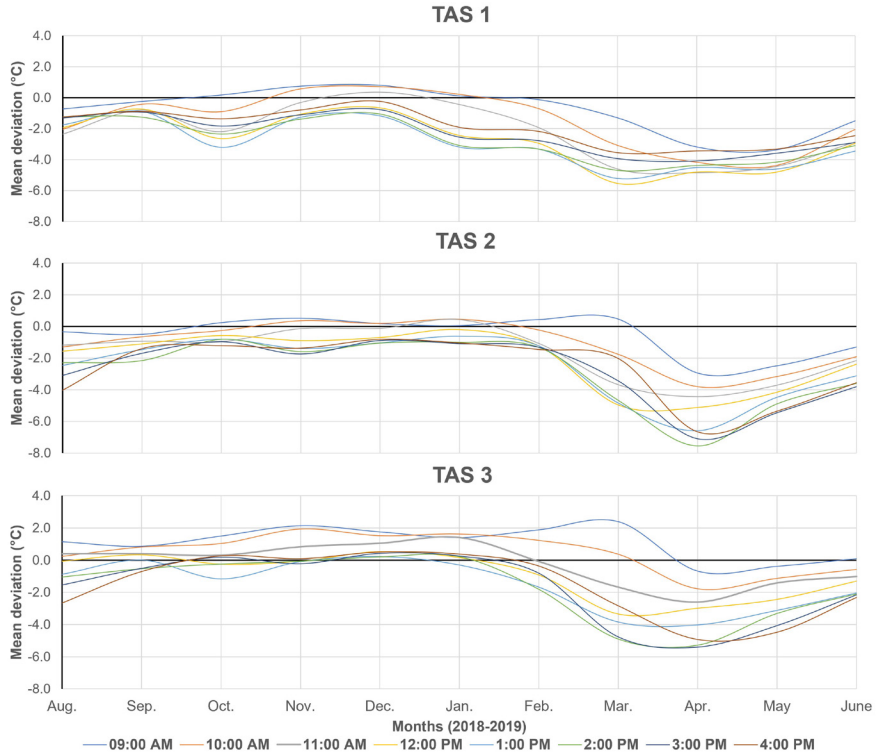

Fig. 10 - Monthly mean deviation for the period 2018-2019, by hour, calculated between the corrected air temperature from weather stations and the automatic time-lapse cameras.

A negative mean deviation value indicates that the automatic time-lapse camera overestimated the air temperature value corrected from the weather station.

Fig. 1 - Moyennes mensuelles des écarts de températures pour la période 2018-2019, par heure, entre les températures corrigées des stations météorologiques et les appareils photographiques automatisés.

Une valeur négative de l'écart exprime une surestimation des températures faites par l'appareil photographique automatisé.

Also consistent with the previous year, T_{cam} were less accurate at the beginning of March, as mean deviation values rose to –4.0°C on average for TAS 1, –3.1°C for TAS 2, and –2.3°C for TAS 3. The accuracy of temperature measurements continued to decline in April, when all three cameras had poorer overall performances: –4.2°C (TAS 1), –5.5°C (TAS 2), and –3.5°C (TAS 3). From March to May, the greatest mean standard deviation values were observed, reaching a maximum of ± 3.8 in March for both TAS 1 and TAS 2. Beginning in June, the accuracy of T_{cam} started to progressively improve, with mean deviations getting closer to 0°C, and the mean standard deviation values also.

1.2. Hourly scale

At the hourly scale, results were very similar to those observed in 2017-2018. The cameras were better at measuring temperature early in the day (9:00 AM - 11:00 AM) as compared to the afternoon (12:00 PM - 3:00 PM) (fig. 11C). Just like the previous year, cameras TAS 1 and TAS 2 performed better at 9:00 AM, respectively over-estimating temperature. Moreover, both cameras improved at 9:00 AM when compared to the first year's data (improvement of 0.5°C for TAS 1 and 0.4°C for TAS 2). The TAS 3 camera mostly under-estimated temperature between 9:00 AM and 10:00 AM, as shown by the positive mean deviation values. The mean deviation value was even closer to 0°C at 11:00 AM, when it generally over-estimated temperature (–0.2°C). It was also between 9:00 AM and 11:00 AM that mean standard deviation values were the lowest, with a minimum value of ± 1.5°C at 11:00 AM for the TAS 3 camera (Figure 2D).

The most significant mean deviations were again observed during the afternoon for all three cameras. The hour at which TAS 1 camera was the least accurate at 1:00 PM which is an hour earlier than during the 2017-2018 period. Both the TAS 2 and TAS 3 cameras were also less accurate an hour earlier than on the year before. They showed the greatest deviations at 2:00 PM, which contrasts with 3:00 PM in 2017-2018. The afternoon was also the period when mean standard deviation values peaked for all three cameras.

2. The 2019-2020 period

At the beginning of October 2019, a fourth Reconyx Hyperfire PC 800 camera was added within the Tasiapik Valley area to document snow-avalanche events on another possible track (TAS 4). We compared T_{cam} recorded by this fourth camera with

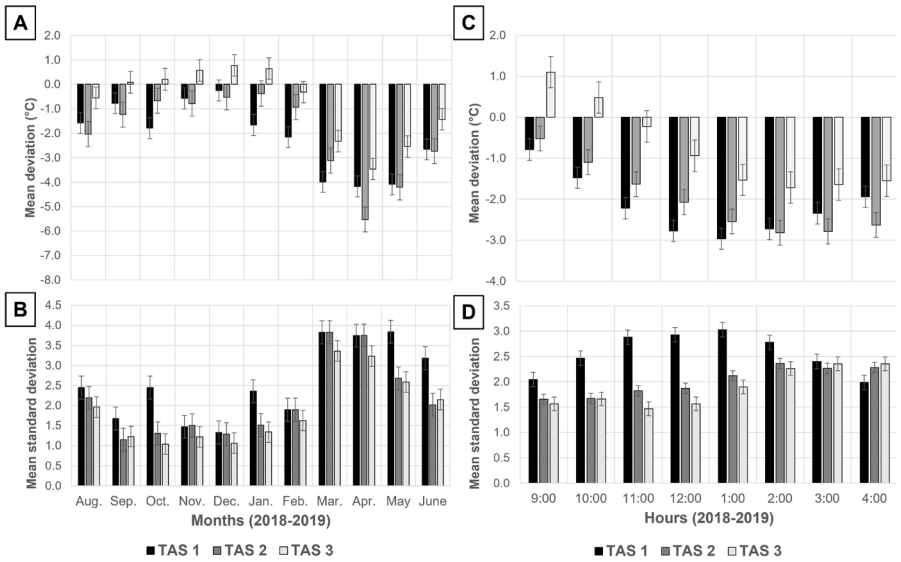

Fig. 11 - Monthly and hourly mean deviations and mean standard deviations of air temperature registered by automatic time-lapse cameras in comparison with air temperature values corrected from the weather stations in 2018-2019.

A: Monthly mean deviations; B: Monthly mean standard deviations; C: Hourly mean deviations; D: Hourly mean standard deviations.

Fig. 11 - Écarts mensuels moyens, horaires moyens, et écarts-types relevés entre les valeurs de températures enregistrées par les appareils photographiques automatisés et les valeurs de températures corrigées des stations météorologiques en 2018-2019.

A : Écarts mensuels moyens ; B : Écarts types mensuels ; C : Écarts horaires moyens ; D : Écart type horaire.

T_{wsc}. No data was collected by the TAS 4 camera before October 6th, 2019, at 4:00 PM.

The results for the 2019-2020 study period were alike those of the two previous years. The sinusoidal-like shape of the mean deviation curves was again visible for every camera-station pairing (fig. 12). The yearly mean deviation between temperature registered by the cameras and the corrected temperature values from the weather stations was once again a negative value for every pairing, highlighting the fact that T_{cam} mostly over-estimate T_{wsc}. The TAS 3 camera was the one that performed best at temperature measurement. TAS 2, TAS 1, and the newly installed TAS 4 cameras had mean deviations of –1.9°C, –2.0°C and –2.3°C respectively.

2.1. Monthly scale

Between September 1st 2019, and June 30th 2020, similar patterns than in the previous years were observed for the TAS 1, TAS 2 and TAS 3 cameras. In fact, T_{cam} were quite reliable from September to February, as the mean deviations remained mostly below ± 2°C (fig. 13A). During the 2019-2020 study period, the TAS 1 and TAS 4 cameras were most accurate in October, with respective average deviations of –0.1°C and –0.7°C with VDTSILA weather station. The TAS 3 camera performed better in September (+0.14°C deviation on average), while the TAS 2 camera had its best result in December, with a mean deviation of –0.4°C as compared to the VDTSILA station. It was also during the period from September to February that the lowest standard deviation values were observed, computed at ± 2.5 throughout this period (fig. 13B).

In 2019-2020, T_{cam} became less accurate in March and this trend continued for the rest of this period. The TAS 3 camera tended to under-estimate temperature between October and February, as shown by the positive deviation values with the weather station, until it began to over-estimate them in March, which was also a notable characteristic during the previous years. All the cameras were the least accurate in April. The camera that was the least accurate overall was the TAS 2 camera, with an average deviation of –5.2°C, followed by TAS 4, with an average deviation of –4.5°C. The TAS 1 camera then followed with an average deviation of –4.0°C. The TAS 3 camera performed better than the three other cameras, with an average deviation of –3.3°C. The standard deviation values were greatest for TAS 2 (± 3.15), TAS 3 (± 2.60) and TAS 4 (± 2.23) in April, whereas the greatest standard deviation value was observed in February for the TAS 1 camera.

2.2. Hourly scale

During the 2019-2020 period, we observed that for all the four cameras T_{cam} were better at before noon than in the afternoon (fig. 12C). In fact, before noon, the average deviation between T_{cam} and T_{wsc} was generally below 2°C, except for the TAS 1 camera at 11:00 AM (–2.1°C). Three of the four cameras performed best at 09:00 AM. These were TAS 2 (average deviation of –0.7°C), TAS 1 (average deviation of –1.1°C), and TAS 4 (average deviation of –1.2°C). The TAS 3 camera underestimated temperatures at 09:00 AM (+0.9°C) and at 10:00 AM (+0.5°C), but performed best at 11:00 AM, with an average deviation of –0.2°C in comparison with values from VDTSILA weather station.

The greatest deviations in temperature measurements by cameras occurred during the afternoon for all four cameras. The TAS 1 camera showed the greatest deviation at 1:00 PM and showed an average deviation of –2.4°C from the UMIROCA weather station. The TAS 2 camera had its worst performances at 3:00 PM, with an average deviation of –2.8°C. The TAS 3 camera's greatest deviations from T_{wsc} were also observed at 3:00 PM and 4:00 PM, with average deviation of –1.6°C. The newly installed TAS 4 camera also performed worse during the afternoon, especially at 2:00 PM and 3:00 PM, with similar mean average deviations of –2.9°C. These negative deviation values reveal the tendency of T_{cam} to over-estimate temperature during the afternoon in comparison with data from the weather stations (fig. 13D) and confirm the observations of the two previous years.

3. Impacts of downwelling shortwave radiation on the accuracy of time-lapse cameras at temperature measurement 2018-2019

Results of the period of 2018-2019 were very similar to those of the period 2017-2018, further highlighting the effects of solar

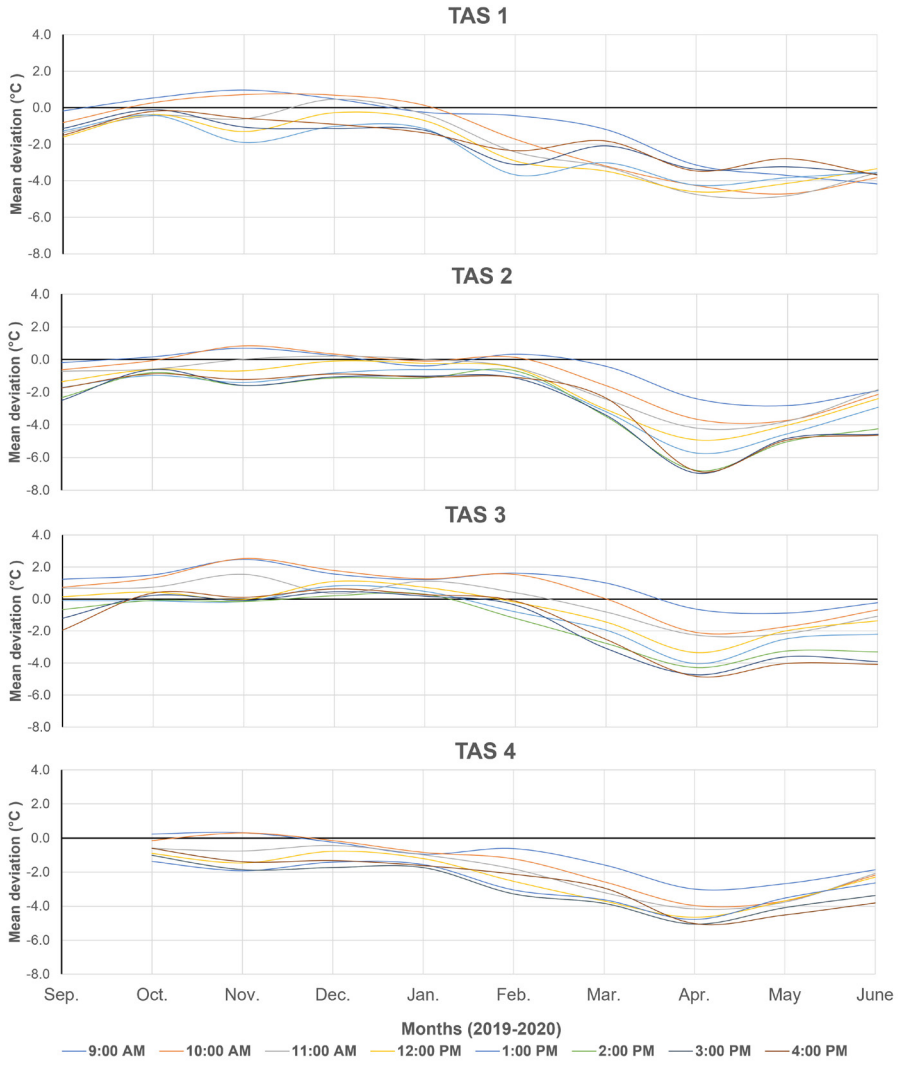

Fig. 12 - Monthly mean deviation for the period 2019-2020, by hour, calculated between the corrected air temperature from weather stations and the automatic time-lapse cameras.

A negative mean deviation value indicates that the automatic time-lapse camera overestimated the air temperature value corrected from the weather station.

Fig. 12 - Moyennes mensuelles des écarts de températures pour la période 2019-2020, par heure, entre les températures corrigées des stations météorologiques et les appareils photographiques automatisés.

Une valeur négative de l'écart exprime une surestimation des températures faites par l'appareil photographique automatisé.

irradiance on the precision of time-lapse cameras at temperature measurement (fig. 14A).

Explicitly, during the first two months of the period, the mean downwelling shortwave values reached respectively 332 W/m² in August, and 198 W/m² in September. During these two months, all three cameras again over-estimated air temperatures with calculated mean deviation close to –2°C with T_{wsc}. Thereafter and until late February, time-lapse were more precise at temperature measurement, being rarely more than 1.5°C over or under the air temperature given by weather stations. Again, Figure 14A shows the tendency of TAS 2 to over-estimate air temperature by the mainly negative values in winter, while it also depicts the tendency for TAS 3 to under-estimate air temperature as shown by mean deviation values above 0°C.

From February to June 10th, 2019, time-lapse cameras almost exclusively over-estimated air temperature values highlighting again the importance of solar irradiance on their precision at temperature measurement.

Coefficients of correlation (*R*) also showed strong negative correlation of –0.66 for the TAS 1 camera, –0.76 for the TAS 2 camera, and –0.79 for the TAS 3 camera. Again, according to Cohen's classification (1988) the TAS 1 camera showed a mid-sized effect correlation with daily mean downwelling shortwave, the relationship was however a bit stronger than on the previous year (R^2 = 0.45). Both TAS 2 and TAS 3 showed once again a great effect with daily mean downwelling shortwave (respective R^2 of 0.58 and 0.64) (fig. 14B).

4. Impacts of downwelling shortwave radiation on the accuracy of time-lapse cameras at temperature measurement 2019-2020

The 2019-2020 period data also displayed similar patterns the two previous periods, increasing the probability that the effects of solar irradiation on the precision of time-lapse cameras to measure temperature might not be related to aleatory circumstances (fig. 15A).

During the late autumn and winter months (October to February), when daily mean downwelling shortwave radiation values are at the lowest, the time-lapse cameras were again most accurate at temperature measurement since the mean deviation values remained close to 0°C and only rarely were more than 2°C. Furthermore, the tendency for the TAS 3 time-lapse camera to under-estimate air temperature values in comparison with VDTSILA is still visible by the red line being most of the time over 0°C (fig. 15A).

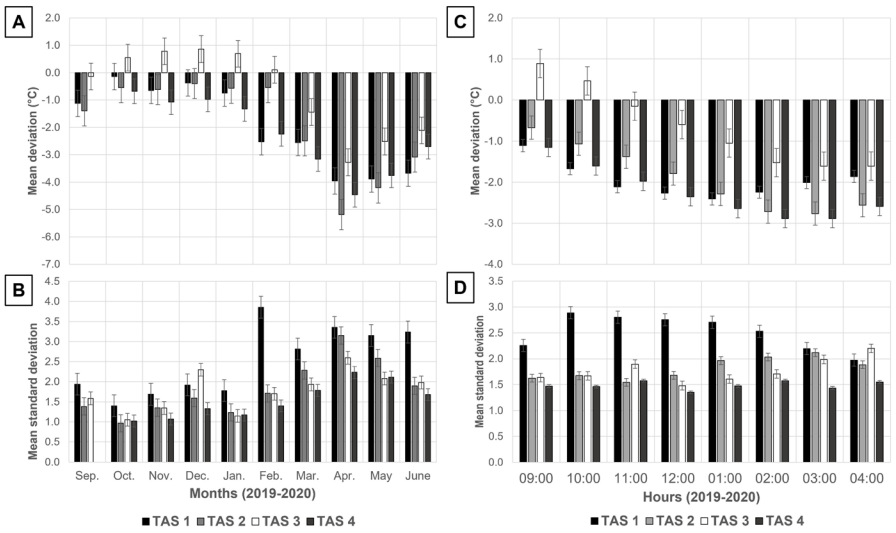

Fig. 13 - Monthly and hourly mean deviations and mean standard deviations of air temperature registered by automatic time-lapse cameras in comparison with air temperature values corrected from the weather stations in 2019-2020.

A: Monthly mean deviations; B: Monthly mean standard deviations; C: Hourly mean deviations; D: Hourly mean standard deviations.

Fig. 13 - Écarts mensuels moyens, horaires moyens, et écarts-types relevés entre les valeurs de températures enregistrées par les appareils photographiques automatisés et les valeurs de températures corrigées des stations météorologiques en 2019-2020.

A : Écarts mensuels moyens ; B : Écarts types mensuels ; C : Écarts horaires moyens ; D : Écarts type horaires (D)

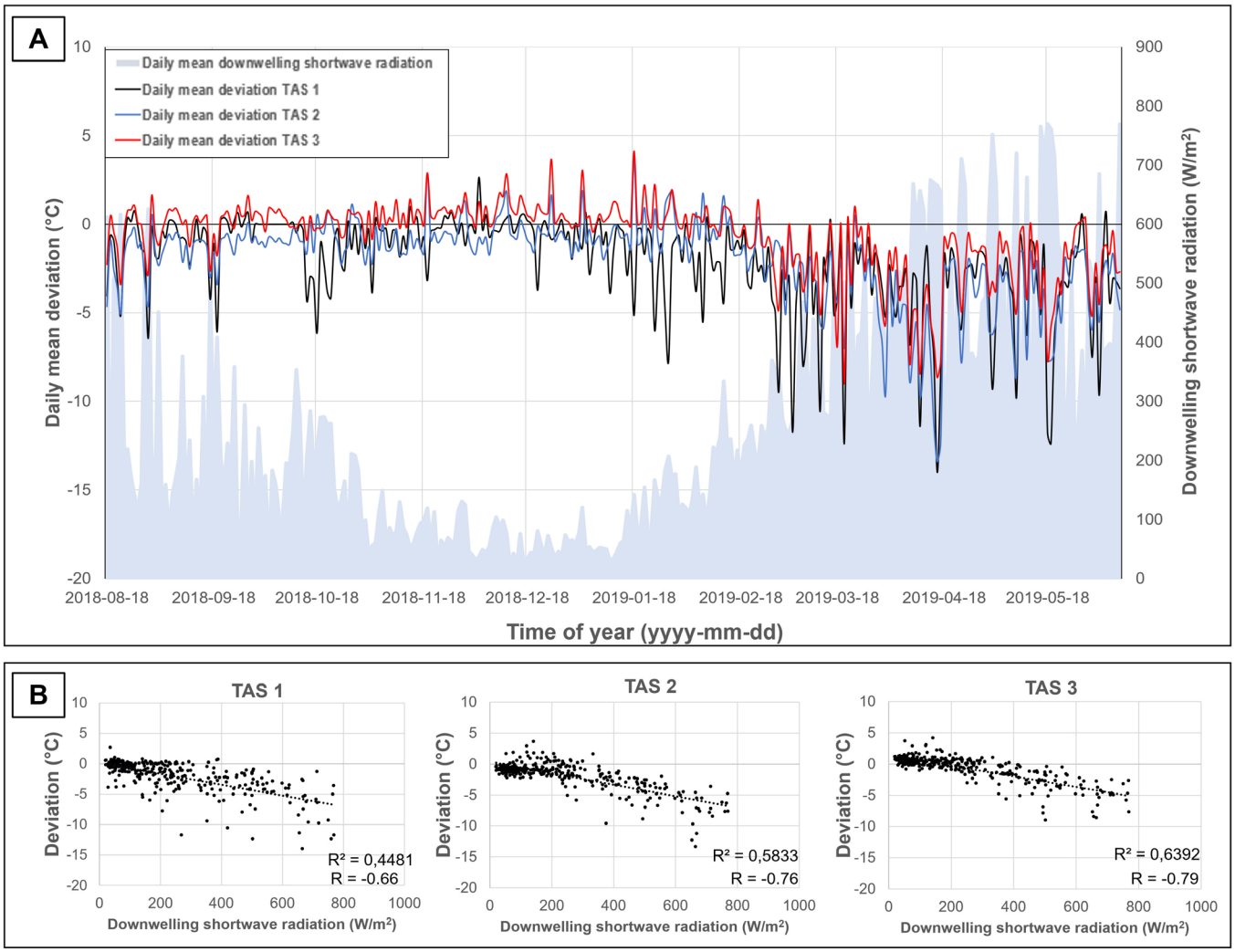

Fig. 14 - Daily mean deviations between air temperature registered on automatic time-lapse cameras and the corrected air temperature values from the weather stations in relationship with downwelling shortwave from August 9th, 2018, to June 10th, 2019 (A); Correlations between daily mean deviations and daily mean downwelling shortwave (B). Data Source: CEN (2020).

Fig. 14 - Valeurs d'écarts journalières entre les valeurs de températures enregistrées par les appareils photographiques automatisés et les stations météorologiques en relation avec la radiation solaire incidente journalière moyenne entre le 9 aout 2018 et le 10 juin 2019 (A) ; Corrélations entre les écarts moyens journaliers observés et la radiation incidente (B). Données Source : CEN (2020).

Coefficients of correlation (R) again all showed strong negative correlation. The coefficients were respectively of −0.67 for the TAS 1 camera, −0.77 for the TAS 2 camera, −0.82 for the TAS 3 camera, and −0.78 for the TAS 4 camera. Once again according to Cohen's classification (1988) of coefficients of determination (R^2), the TAS 1 camera showed a mid-sized effect correlation with daily mean downwelling shortwave (R^2 = 0.46) (fig. 15B). Both TAS 2 and TAS 3 showed great effect with daily mean downwelling shortwave radiation for the third consecutive period (respective R^2 of 0.59 and 0.68). The TAS 4 camera also showed great effect with an R^2 of 0.61.

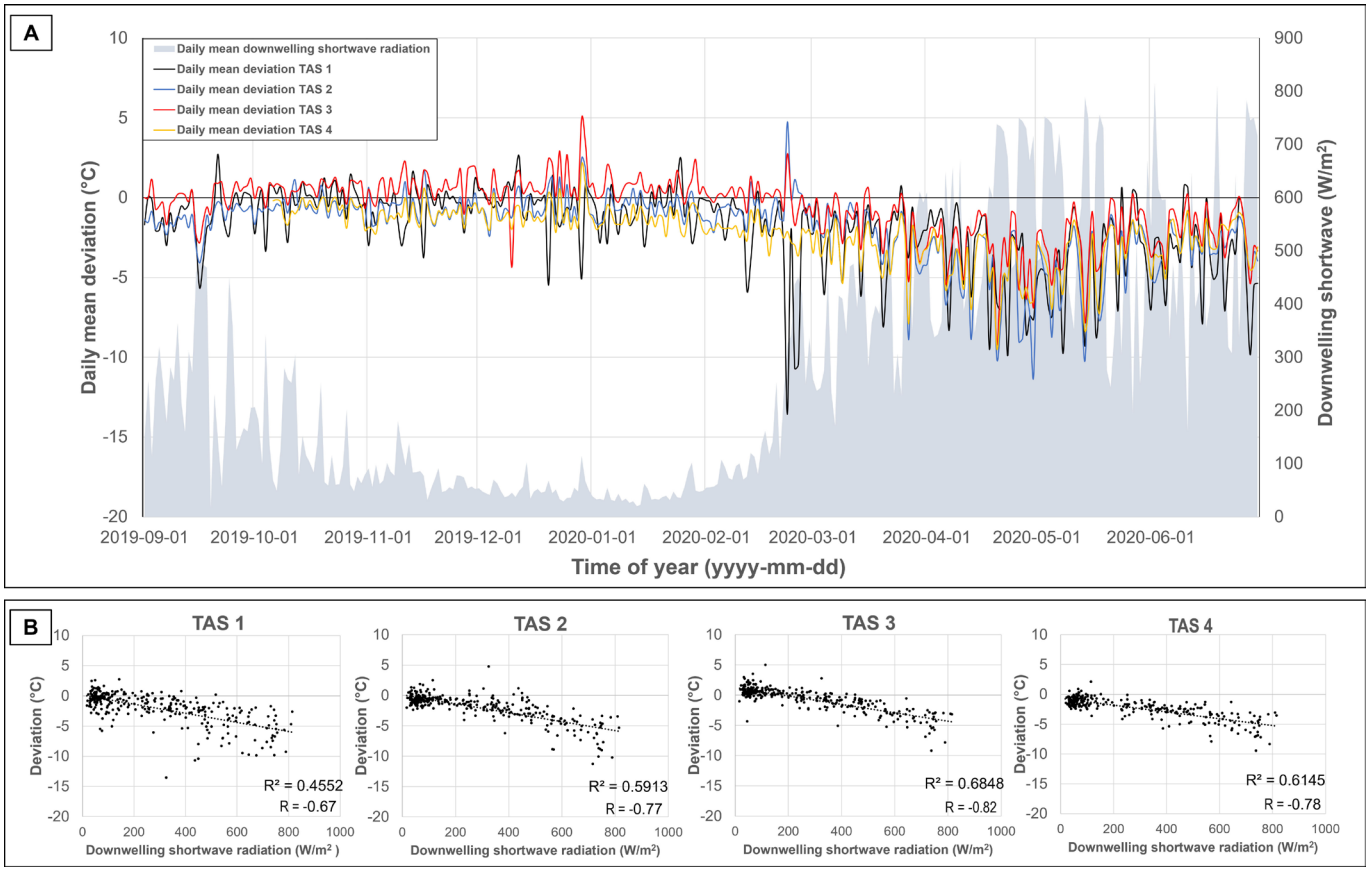

Fig. 15 - Daily mean deviations between air temperature registered on automatic time-lapse cameras and the corrected air temperature values from the weather stations in relationship with downwelling shortwave from September 1st, 2019, to June 30th, 2020 (A); Correlations between daily mean deviations and daily mean downwelling shortwave radiation (B) Data Source: CEN (2020).

Fig. 15 - Valeurs d'écarts journalières entre les valeurs de températures enregistrées par les appareils photographiques automatisés et les stations météorologiques en relation avec la radiation solaire incidente journalière moyenne entre le 1er septembre 2019 et le 30 juin 2020 (A) ; Corrélations entre les écarts moyens journaliers observés et la radiation incidente (B). Données Source : CEN (2020).